

# NPAS1 Represses the Generation of Specific Subtypes of Cortical Interneurons

Amelia Stanco,<sup>1,\*</sup> Ramón Pla,<sup>1,6</sup> Daniel Vogt,<sup>1,6</sup> Yiran Chen,<sup>2</sup> Shyamali Mandal,<sup>1,7</sup> Jamie Walker,<sup>3</sup> Robert F. Hunt,<sup>4</sup> Susan Lindtner,<sup>1</sup> Carolyn A. Erdman,<sup>1</sup> Andrew A. Pieper,<sup>5</sup> Steven P. Hamilton,<sup>1,8</sup> Duan Xu,<sup>2</sup> Scott C. Baraban,<sup>4</sup> and John L.R. Rubenstein<sup>1,\*</sup>

<sup>1</sup>Department of Psychiatry, Neuroscience Program, and the Nina Ireland Laboratory of Developmental Neurobiology, University of California, San Francisco, San Francisco, CA 94158-2324, USA

<sup>2</sup>Department of Radiology and Biomedical Imaging, University of California, San Francisco, San Francisco, CA 94143, USA

<sup>3</sup>Department of Biochemistry, UT Southwestern Medical Center, Dallas, TX 75390, USA

<sup>4</sup>Department of Neurological Surgery, Neuroscience Program, University of California, San Francisco, San Francisco, CA 94143, USA

<sup>5</sup>Department of Psychiatry and Neurology, University of Iowa Carver College of Medicine, Iowa City, IA 52242, USA

<sup>6</sup>Co-second authors

<sup>7</sup>Present address: Genentech, Inc., South San Francisco, CA 94080, USA

<sup>8</sup>Present address: Kaiser Permanente, San Francisco, CA 94118, USA

\*Correspondence: [amelia.stanco@ucsf.edu](mailto:amelia.stanco@ucsf.edu) (A.S.), [john.rubenstein@ucsf.edu](mailto:john.rubenstein@ucsf.edu) (J.L.R.R.)

<http://dx.doi.org/10.1016/j.neuron.2014.10.040>

## SUMMARY

Little is known about genetic mechanisms that regulate the ratio of cortical excitatory and inhibitory neurons. We show that *NPAS1* and *NPAS3* transcription factors (TFs) are expressed in progenitor domains of the mouse basal ganglia (subpallium, MGE, and CGE). *NPAS1*<sup>−/−</sup> mutants had increased proliferation, ERK signaling, and expression of *Arx* in the MGE and CGE. *NPAS1*<sup>−/−</sup> mutants also had increased neocortical inhibition (sIPSC and mIPSC) and generated an excess of somatostatin<sup>+</sup> (SST) (MGE-derived) and vasoactive intestinal polypeptide<sup>+</sup> (VIP) (CGE-derived) neocortical interneurons, but had a normal density of parvalbumin<sup>+</sup> (PV) (MGE-derived) interneurons. In contrast, *NPAS3*<sup>−/−</sup> mutants showed decreased proliferation and ERK signaling in progenitors of the ganglionic eminences and had fewer SST<sup>+</sup> and VIP<sup>+</sup> interneurons. *NPAS1* repressed activity of an *Arx* enhancer, and *Arx* overexpression resulted in increased proliferation of CGE progenitors. These results provide insights into genetic regulation of cortical interneuron numbers and cortical inhibitory tone.

## INTRODUCTION

While rapid progress has been made in understanding the regulation of neural regional and cell fate specification, much less is known about genetic mechanisms underlying brain size and how the correct ratios of excitatory and inhibitory neurons within local circuits are generated. Understanding these mechanisms is essential for elucidating important facets of brain development that underlie neurodevelopmental disorders that may have an imbalance of cortical excitation/inhibition (E/I) (e.g., epilepsy,

autism spectrum disorders [ASDs], and schizophrenia) (Lewis et al., 2012; Marín, 2012; Rubenstein and Merzenich, 2003; Yizhar et al., 2011), and to understanding why many autistic children have macrocephaly that includes a large cerebral cortex (Courchesne et al., 2007; Hazlett et al., 2011). While unifying genetic mechanisms which control cortex size and E/I balance have not yet been elucidated, progress has been made in understanding each of these processes individually.

Genetic causes of human neonatal macrocephaly are present in individuals with mutations in genes regulating growth factor signaling, particularly in pathways that engage the function of AKT and PTEN (Poduri et al., 2012; Rivière et al., 2012; Striano and Zara, 2012; Zhou and Parada, 2012), and RAS and MAPK (Gripp et al., 2013). For instance, patients who are heterozygotes for loss-of-function PTEN mutations have macrocephaly and are at increased risk for autism (Zhou and Parada, 2012).

Likewise, progress has been made in understanding the mechanisms that control the generation of cortical excitatory and inhibitory neurons (Gelman et al., 2012; Kwan et al., 2012; Marín, 2013) and the mechanisms that coordinate their relative activities to create the proper E/I balance (Le Magueresse and Monyer, 2013). In this regard, there is particular interest in the mechanisms that control the development of cortical inhibitory neurons (GABAergic interneurons). In rodents, most cortical inhibitory neurons are generated during embryogenesis in subpallial structures called the caudal and medial ganglionic eminences (CGEs and MGEs) (Rudy et al., 2011).

The specification, migration, and differentiation of cortical interneurons are controlled by cascades of transcription factors (TFs). Some TFs regulate the development of either CGE- or MGE-derived neurons. For instance, *Lhx6*, *Nkx2-1*, *Olig1*, and *Sox6* regulate for the specification and differentiation of MGE-derived interneurons (Azim et al., 2009; Batista-Brito et al., 2009; Liodis et al., 2007; Silbereis et al., 2014; Sussel et al., 1999; Zhao et al., 2008). Other TFs, such as the *Arx* and *Dlx* genes, control development of both CGE- and MGE-derived interneurons (Cobos et al., 2005; Colasante et al., 2008; Marsh et al., 2009).

Herein, we present evidence that the mouse *NPAS* basic helix-loop-helix (bHLH)-PAS TF genes (Erbel-Sieler et al., 2004; Pieper et al., 2005; Zhou et al., 1997) are regulators of cortex size and E/I balance. *NPAS1* and *NPAS3* are expressed in telencephalic progenitor domains of the cortex, and the CGE and MGE, and later in immature and mature cortical interneurons (Batista-Brito et al., 2008; Erbel-Sieler et al., 2004; Zhao et al., 2008). Vertebrate *NPAS* function in embryonic neural progenitors may be related to the function of *Trachealess*, the *NPAS Drosophila* homolog. *Trachealess* modulates fibroblast growth factor (FGF) signaling by transcriptional regulation of the FGF receptor (Ohshiro and Saigo, 1997). In the adult mouse hippocampus, *NPAS3* regulates expression of *FGFR1* to control proliferation of hippocampal granule neurons (Pieper et al., 2005). Here, we have found that *NPAS1* negatively regulates proliferation and MAPK signaling in CGE and MGE progenitors, not by regulating FGF receptor expression but through an unexpected mechanism, repression of *Arx* expression. As a result, *NPAS1*<sup>−/−</sup> mutants generated excessive cortical interneurons prenatally, which persisted into adulthood. *NPAS1*<sup>−/−</sup> mutants also had increased neocortical inhibition (sIPSC and mIPSC) and generated an excess of SST<sup>+</sup> (MGE-derived) and VIP<sup>+</sup> (CGE-derived) neocortical interneurons, but had normal numbers of PV<sup>+</sup> (MGE-derived) interneurons. In contrast, *NPAS3*<sup>−/−</sup> mutants had a complementary phenotype, with reduced proliferation and MAPK signaling in progenitors of the ganglionic eminences, and the postnatal cortex had fewer SST<sup>+</sup> and VIP<sup>+</sup> interneurons.

We propose that our analysis of *NPAS1* and *NPAS3* functions in mice provides mechanistic insights into human neuropsychiatric disorders, as *NPAS3* dysfunction is implicated in schizophrenia (Kamnasaran et al., 2003; Macintyre et al., 2010). Furthermore, we have identified sporadic nonsynonymous mutations in *NPAS1* and *NPAS3* in autistic individuals.

## RESULTS

### *NPAS1* and *NPAS3* Expression during Interneuron Development

The subpallium generates neocortical interneurons (Flandin et al., 2011; Marín, 2012; Rudy et al., 2011). We examined *NPAS1* and *NPAS3* RNA expression by in situ hybridization (ISH) at E13.5, E15.5, and P5 (Figure 1) and assessed *NPAS1* and *NPAS3* expression by immunofluorescence at P0, P5, P15, and P30 (Figure 1, and see Figures S1 and S2 and Tables S1 and S2 available online). At E13.5, both had pallial and subpallial ventricular zone (VZ) expression. *NPAS1* showed notable expression in the VZ and subventricular zone (SVZ) of the dorsal and ventral MGE, and CGE. By E15.5, *NPAS3* was expressed in the MGE mantle zone; *NPAS1* expression was prominent in the pallial and subpallial SVZ.

Previous studies have described coexpression of *NPAS1* or *NPAS3* with cortical interneurons using GABA, GAD-67, or calretinin antibodies in the adult mouse brain (Erbel-Sieler et al., 2004). We have extended coexpression analysis of *NPAS1* or *NPAS3* with various interneuron markers during cortical interneuron development and in the adult (Figures 1, S1, and S2; Tables S1 and S2). At P0, *NPAS1* was expressed in neocortical interneurons; ~100% of *NPAS1*<sup>+</sup> cells express *GAD67-GFP*; ~30%

had MGE-like properties (*Lhx6-GFP*<sup>+</sup>) (Figures 1D, 1F, S1A, and S1B). By P5, *NPAS1* and *NPAS3* were expressed in rostro-caudal gradients in neocortical interneurons; we are unaware of other TFs with this property. Virtually all neocortical *NPAS1*<sup>+</sup> cells (99% ± 0.29%) and the majority of *NPAS3*<sup>+</sup> cells (67% ± 2.94%) expressed *GAD67-GFP* at P5 (Figures S1C and S1D). By P15, *NPAS1* and *NPAS3* were expressed by a majority of reelin<sup>+</sup> (*NPAS1*, 68% ± 2.78%; *NPAS3*, 79% ± 4.79%) and SST<sup>+</sup> (*NPAS1*, 65% ± 1.95%; *NPAS3*, 75% ± 0.44%) interneurons. Both *NPAS1* and *NPAS3* were expressed in a small proportion of PV<sup>+</sup> cells (*NPAS1*, 6% ± 0.85%) (*NPAS3*, 13% ± 1.29%) (Figures S1E, S1F, S1H–S1J, and S1L). At P30, *NPAS1*<sup>+</sup> cells coexpressed reelin, SST, calretinin (CR), or neuropeptide Y (NPY) but rarely coexpressed PV (reelin, 42% ± 1.94%; SST, 36% ± 3.72%; CR, 28% ± 2.89%; NPY, 12% ± 0.70%; PV, 5% ± 1.24%). On the other hand, *NPAS3*<sup>+</sup> was expressed in a large fraction of all interneuron subtypes assayed, including PV (reelin, 74% ± 2.31%; SST, 75% ± 3.52%; CR, 51% ± 1.23%; PV, 43% ± 1.40%) (Figures S2B–S2E and S2G–S2J; data not shown).

### Increased Numbers of Neocortical Interneurons in *NPAS1*<sup>−/−</sup> Mutants

We studied the effect of an *NPAS1* null allele (*NPAS1*<sup>−/−</sup>) (Erbel-Sieler et al., 2004) on neocortical interneuron development using a *GAD67-GFP* allele to label all of the interneurons (Tamamaki et al., 2003). By E15.5 there was an increased density of GFP<sup>+</sup> interneurons through the intermediate zone and then throughout the cortical wall at E17.5 and P0 (26%–41%; E15.5, 26% ± 4.67%, *p* = 0.00099; E17.5, 35% ± 2.08%, *p* = 9.08E-8; P0, 41% ± 4.46%, *p* = 2.48E-6) (Figures 2A–2C and 2E–2G). Even though there was ~2-fold increased interneuron cell death at P7 (activated caspase-3, Figures S3A and S3B), P30 mice maintained ~15% (15% ± 5.43%, *p* = 0.044) more interneurons (Figures 2D and 2H). Surprisingly, while SST<sup>+</sup>, VIP<sup>+</sup>, NPY<sup>+</sup>, and reelin<sup>+</sup> interneuron subtypes were increased (28%–44%; SST, 32% ± 5.07%, *p* = 0.001; VIP, 44% ± 7.99%, *p* = 0.014; NPY, 34% ± 7.42%, *p* = 0.0019; reelin, 28% ± 3.01%, *p* = 2.7E-5), PV<sup>+</sup> interneuron density was normal (Figures 3A–3E, 3A'–3E', and 3F–3J). MRI quantification showed that P30 cortical volume was increased 10% (10% ± 1.40%, *p* = 0.0055) (Figures S3F and S3G; Table S3). Nissl section analysis supported the MRI findings, and showed 11% increased (11% ± 3.13%, *p* = 0.03) rostral neocortical width (Figures S2A and S2B). Assessment of NeuN<sup>+</sup> (neuronal marker) cells in the P21 somatosensory cortex suggests that the enhancement in cortical volume may be the result of increased neuron numbers. In *NPAS1*<sup>−/−</sup> mutants, the density of NeuN<sup>+</sup> cells was increased by 11% (cortex, 11% ± 2.21%, *p* = 0.0011; layer I, 22% ± 7.34%, *p* = 0.030; layer IV, 7% ± 2.09%, *p* = 0.025; layer V, 16% ± 3.32%, *p* = 0.0024; layer VI, 13% ± 2.66%, *p* = 0.0052) (Figures S4A and S4B).

### Increased Synaptic Inhibition onto Neocortical Pyramidal Neurons in *NPAS1*<sup>−/−</sup>

To test whether the increase in cortical interneurons altered the physiology of the *NPAS1*<sup>−/−</sup> cortex, we performed patch-clamp recordings of layer II/III somatosensory pyramidal neurons in slices from P21–30 *NPAS1*<sup>−/−</sup> mice and wild-type (WT) littermates (Figures 4A–4C). Compared to WT littermates, pyramidal

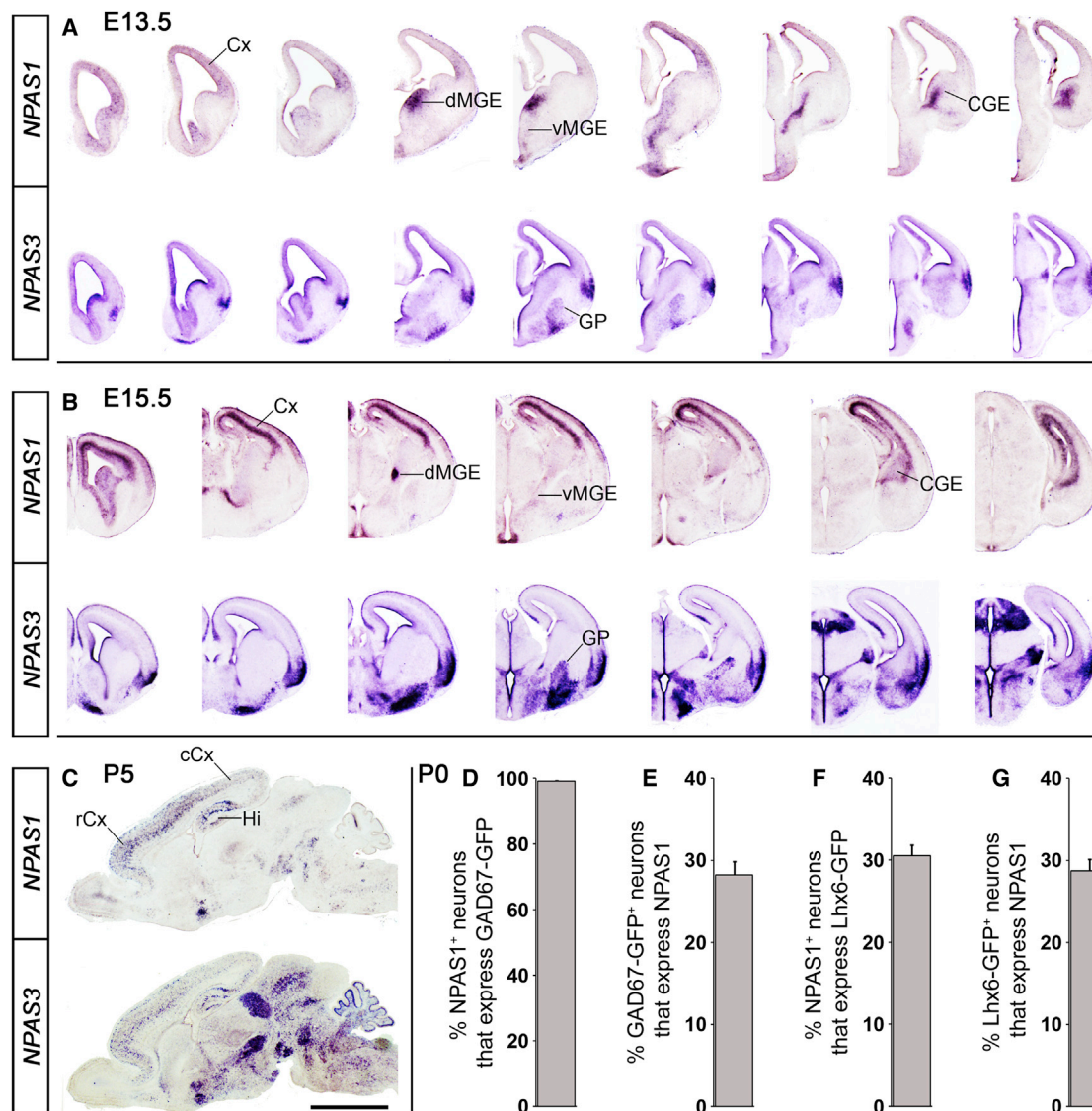


**Figure 1. Forebrain Expression of Mouse *NPAS1* and *NPAS3* during Embryonic and Neonatal Stages**

(A and B) ISH on rostrocaudal series of coronal hemisections at E13.5 (A) and E15.5 (B). Note strong *NPAS1* expression in dMGE and CGE.

(C) ISH on neonatal sagittal sections at P5. Note the rostral bias of cortical expression.

(D–G) Quantification of percentage of *NPAS1*<sup>+</sup> (immuno-stained) cortical interneurons (*GAD67-GFP*<sup>+</sup> and *Lhx6-GFP*<sup>+</sup>) at P0. *n* = 3 animals for (D)–(G). Abbreviations are as follows: CGE, caudal ganglionic eminence; Cx, cortex (rCx, rostral; cCx, caudal); GP, globus pallidus; Hi, hippocampus; MGE, medial ganglionic eminence (dMGE, dorsal; vMGE, ventral). Scale bars, (A) 1.21 mm, (B) 1.74 mm, and (C) 3 mm. See also [Figures S1](#) and [S2](#).

neurons from *NPAS1*<sup>−/−</sup> mice showed an increase in the frequency of spontaneous IPSCs (sIPSCs) (WT,  $8.17 \pm 1.29$  Hz; *NPAS1*<sup>−/−</sup>,  $11.18 \pm 1.26$  Hz;  $p = 0.042$ ). However, the amplitudes and kinetics of inhibitory events were not significantly changed ([Figures 4A](#) and [4B](#)). To further characterize the increase in GABA-mediated synaptic inhibition, tetrodotoxin (TTX) was added to the ACSF to isolate miniature IPSCs (mIPSCs). Similar to spontaneous events, an increase in mIPSC frequencies was observed in *NPAS1*<sup>−/−</sup> mice (WT,  $6.2 \pm 1.24$  Hz; *NPAS1*<sup>−/−</sup>,  $8.74 \pm 1.02$  Hz;  $p = 0.036$ ); amplitudes and kinetics of mIPSCs were not significantly changed ([Figure 4C](#)).

Next, we evaluated the ratio of interneuron numbers to total neuron numbers by quantifying the percentage of NeuN<sup>+</sup> cells (total neurons) that express *GAD67-GFP* in each layer of P21 somatosensory cortex ([Figures S4B](#) and [S4C](#)). At P21, all NeuN<sup>+</sup> cells were *GAD67-GFP*<sup>+</sup> in layer I somatosensory cortex. *NPAS1*<sup>−/−</sup> mutant mice displayed a 19% increase ( $19\% \pm 5.94\%$ ,  $p = 0.025$ ) in *GAD67-GFP*<sup>+</sup> interneurons within layer I ([Figure S4C](#)). In layer II/III, the percentage of NeuN<sup>+</sup> cells that express *GAD67-GFP* was increased by 18% in *NPAS1*<sup>−/−</sup> mutants (*NPAS1*<sup>+/+</sup>,  $27\% \pm 1.13\%$ ; *NPAS1*<sup>−/−</sup>,  $32\% \pm 0.96\%$ ,  $p = 0.0024$ ) ([Figures 4D–4I](#)). We also estimated the excitatory to

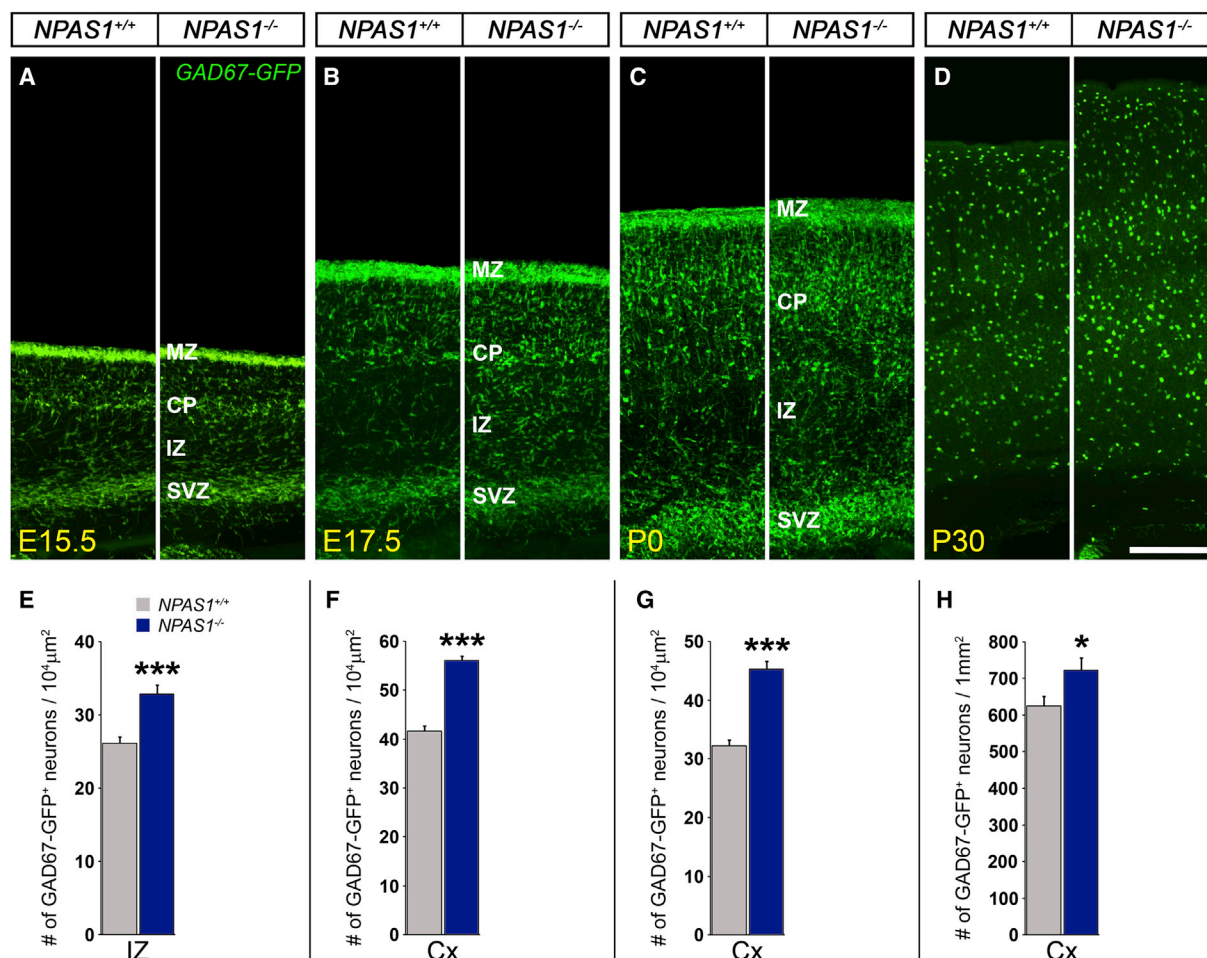


**Figure 2. NPAS1<sup>-/-</sup> Mice Have Increased Numbers and Density of GAD67-GFP<sup>+</sup> Cortical Interneurons**

(A–D) Increase in GAD67-GFP<sup>+</sup> cortical interneurons (somatosensory Cx) beginning by E15.5 shown on coronal cortical sections at E15.5 (A), E17.5 (B), P0 (C), and P30 (D) in NPAS1<sup>-/-</sup> mice.

(E–H) Quantification of GAD67-GFP<sup>+</sup> neurons/10<sup>4</sup> μm<sup>2</sup> at E15.5 (E), E17.5 (F), P0 (G), and GAD67-GFP<sup>+</sup> neurons/1 mm<sup>2</sup> at P30 (H). n = 3 animals per genotype for (E)–(H). Abbreviations are as follows: CP, cortical plate; Cx, cortex; IZ, intermediate zone; MZ, marginal zone; SVZ, subventricular zone. \*p < 0.05. \*\*\*p < 0.001. Scale bars, (A)–(C), 200 μm; (D), 400 μm. See also Figure S3.

inhibitory cell ratio (E/I) in each cortical layer at P21. The E/I ratio, determined as the ratio of NeuN<sup>+</sup> and GAD67<sup>+</sup> cells to GAD67<sup>+</sup> cells, was decreased by 23% in layer II/III of the NPAS1<sup>-/-</sup> somatosensory cortex (NPAS1<sup>+/+</sup>, 2.74 ± 0.17; NPAS1<sup>-/-</sup>, 2.12 ± 0.091, p = 0.0040) (Figure S4D). No significant change in the E/I cell ratio was found in deep cortical layers (IV, V, or VI) (Figure S4D). These findings were supported by stereological quantification of NeuN<sup>+</sup> and GAD67<sup>+</sup> cells within the cerebral cortex. The NPAS1<sup>-/-</sup> mutant cerebral cortex exhibited a 35% increase (35% ± 5.96%, p = 0.0053) in NeuN<sup>+</sup> cells and a 57% increase (57% ± 10.49%, p = 0.0012) in GAD67<sup>+</sup> cells at 3 months of age (Figures S4E–S4G). Cortical pyramidal cell density was unchanged in P21 NPAS1<sup>-/-</sup> mutants as indicated by Cux1<sup>+</sup>, Ctip2<sup>+</sup>, and Tbr1<sup>+</sup> immunofluorescence staining which labels layer II/III, layer V, and layer VI, respectively (Figures S4H–S4K). Thus, the enhanced level of synaptic inhibition onto layer II/III neocortical pyramidal neurons

in the NPAS1<sup>-/-</sup> mutant was associated with an increased fraction of inhibitory neurons.

### NPAS1<sup>-/-</sup> and NPAS3<sup>-/-</sup> Had Opposite Effects on Cortical Interneuron Numbers

NPAS3<sup>-/-</sup> mice display reduced proliferation and size of the adult hippocampal dentate gyrus (Pieper et al., 2005). Given that NPAS1<sup>-/-</sup> mutants have increased cortical volume (Figures S3F and S3G) and interneuron numbers (Figures 3A–3C, 3E, 3A'–3C', 3E', 3F–3H, and 3J), we hypothesized that NPAS1 and NPAS3 may have opposing functions on interneuron development. Therefore, we compared interneuron numbers in NPAS1<sup>-/-</sup>, NPAS3<sup>-/-</sup>, and NPAS1/3<sup>-/-</sup> P30 neocortices. While NPAS1<sup>-/-</sup> mutants had increased density of cortical interneurons (Figures 3A–3C, 3E, 3A'–3C', 3E', 3F–3H, and 3J), NPAS3<sup>-/-</sup> mutants had reduced density of SST<sup>+</sup>, VIP<sup>+</sup>, NPY<sup>+</sup>, and reelin<sup>+</sup> interneurons (Figures 3A–3C, 3E, 3A'–3C', 3E',

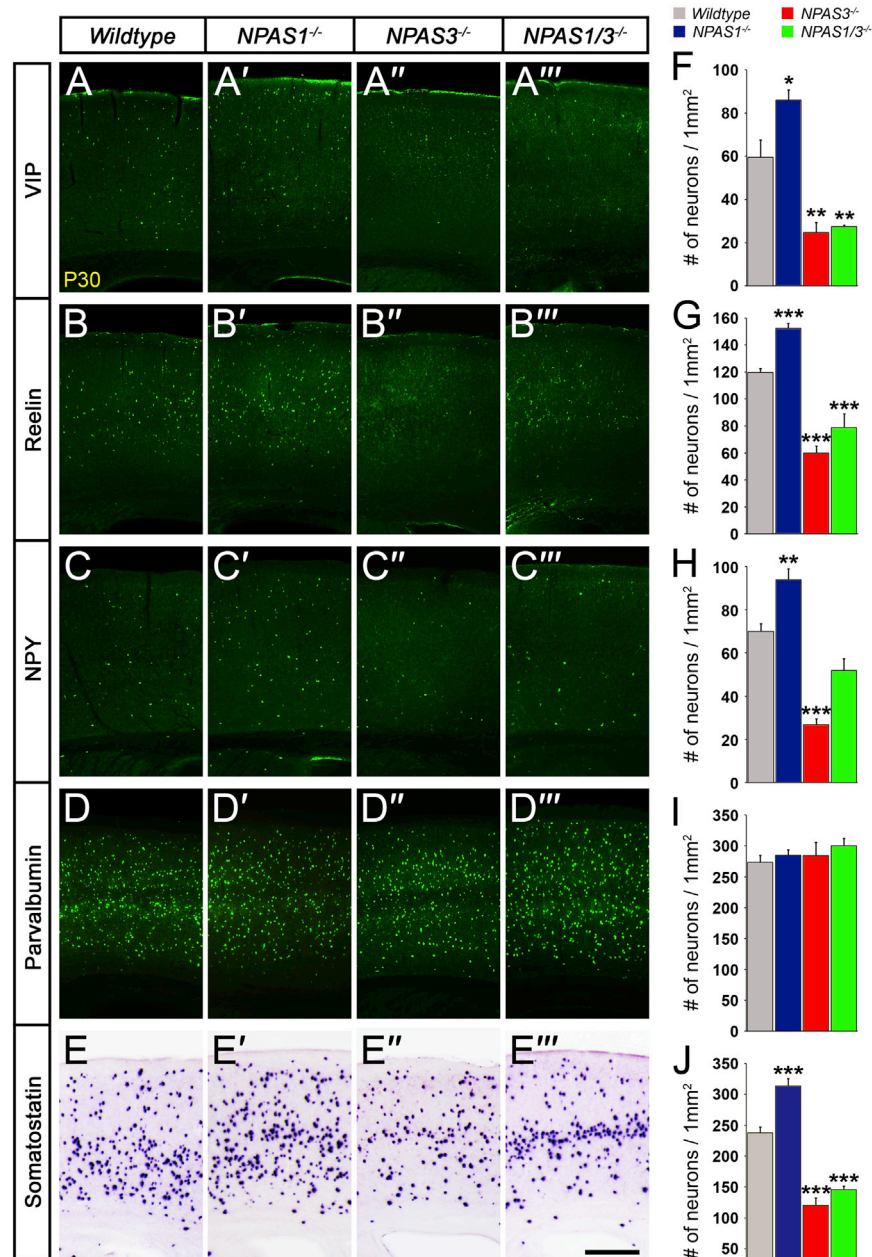


**Figure 3. NPAS1<sup>-/-</sup> Mice Have Increased, whereas NPAS3<sup>-/-</sup> and NPAS1/3<sup>-/-</sup> Mice Have Decreased, Cortical Interneurons**

(A–E''') Interneurons expressing VIP, reelin, NPY, and somatostatin are increased in NPAS1<sup>-/-</sup> mice but decreased in NPAS3<sup>-/-</sup> and NPAS1/3<sup>-/-</sup> mice. All mutants have a normal density of parvalbumin<sup>+</sup> interneurons. Immunofluorescence staining of coronal neocortical sections (somatosensory Cx) at P30.

(F–J) Quantification of VIP<sup>+</sup> (F), reelin<sup>+</sup> (G), NPY<sup>+</sup> (H), parvalbumin<sup>+</sup> (I), and somatostatin<sup>+</sup> (J) neurons/mm<sup>2</sup>. n = 3 animals per genotype for (F)–(J). \*p < 0.05. \*\*\*p < 0.001. Scale bar, (A)–(E''') 400 μm.

In addition, we observed probable NPAS1<sup>-/-</sup>, NPAS3<sup>-/-</sup>, and NPAS1/3<sup>-/-</sup> mutant basal ganglia phenotypes (n = 1), which include subtle cholinergic defects (NPAS1 and NPAS3 are expressed in the pallidum) (Figure 1 and data not shown) (Flandin et al., 2010; Nóbrega-Pereira et al., 2010). The distribution of choline acetyltransferase (ChAT)<sup>+</sup> cells around the globus pallidus (GP) was abnormal in NPAS1/3<sup>-/-</sup> and NPAS3<sup>-/-</sup> mutants. We detected increased ChAT<sup>+</sup> cells inside the GP and reduced numbers in the ventral pallidum. While parvalbumin (PV)<sup>+</sup> expression in the GP was not grossly abnormal in the mutants, the GP may be enlarged in the NPAS1<sup>-/-</sup> mutant and smaller in the NPAS3<sup>-/-</sup> mutant. PV<sup>+</sup> interneuron numbers in the striatum and basolateral nucleus of the amygdala appeared grossly normal in all three mutant genotypes (data not shown).

### NPAS1<sup>-/-</sup> and NPAS3<sup>-/-</sup> Ganglionic Eminences Had Opposite Proliferation and ERK-Signaling Phenotypes

Given that NPAS1 and NPAS3 are expressed in MGE and CGE progenitors (Figures 1A and 1B), we explored whether changes in interneuron numbers in

3F–3H, and 3J). Like NPAS1<sup>-/-</sup> mutants, there was not a change in the density of PV<sup>+</sup> interneurons (Figures 3D–3D'' and 3I).

MRI quantification revealed that P30 cortical volume was increased in NPAS1<sup>-/-</sup> mutant mice, as opposed to a 21% decrease (21% ± 1.47%, p = 0.0039) in NPAS3<sup>-/-</sup> mutants. Also, we found differential changes in P30 NPAS1<sup>-/-</sup> and NPAS3<sup>-/-</sup> mutant basal ganglia volumes by MRI. NPAS1<sup>-/-</sup> mutant mice displayed a 12% increase (12% ± 1.74%, p = 0.042) and NPAS3<sup>-/-</sup> mutants a 25% decrease (25% ± 2.24%, p = 0.0087) in basal ganglia volume (Figures S3F–S3H; Table S3).

NPAS1/3<sup>-/-</sup> and NPAS3<sup>-/-</sup> mutants had similar interneuron phenotypes (Figures 3A–3E, 3A''–3E'', 3A'''–3E''', and 3F–3J).

NPAS1<sup>-/-</sup> and NPAS3<sup>-/-</sup> mutants were due to changes in proliferation using a marker of M phase cells (phosphohistone H3, PH3). We found that NPAS1<sup>-/-</sup> mutants had a 1.6-fold increase (1.61 ± 0.13, p = 0.0007) in PH3<sup>+</sup> cells in the VZ, and a 1.3-fold increase (1.31 ± 0.039, p = 0.0033) in the SVZ of the CGE at E13.5; at E15.5 NPAS1<sup>-/-</sup> mutants had a 1.3-fold increase (VZ, 1.32 ± 0.042, p = 1.09E-5; SVZ, 1.30 ± 0.035, p = 0.022) in PH3<sup>+</sup> cells in the VZ and SVZ of the MGE (Figures 5A, 5B, 5E, 5F, 5I, and 5K). In contrast, NPAS3<sup>-/-</sup> progenitors displayed reduced proliferation in the E13.5 MGE, including a 1.3-fold decrease (1.26 ± 0.043, p = 0.010) in PH3<sup>+</sup> cells in the VZ and a 1.4-fold decrease (1.44 ± 0.031, p = 6.54E-5) in the SVZ (Figures 5Q, 5R, and 5W).

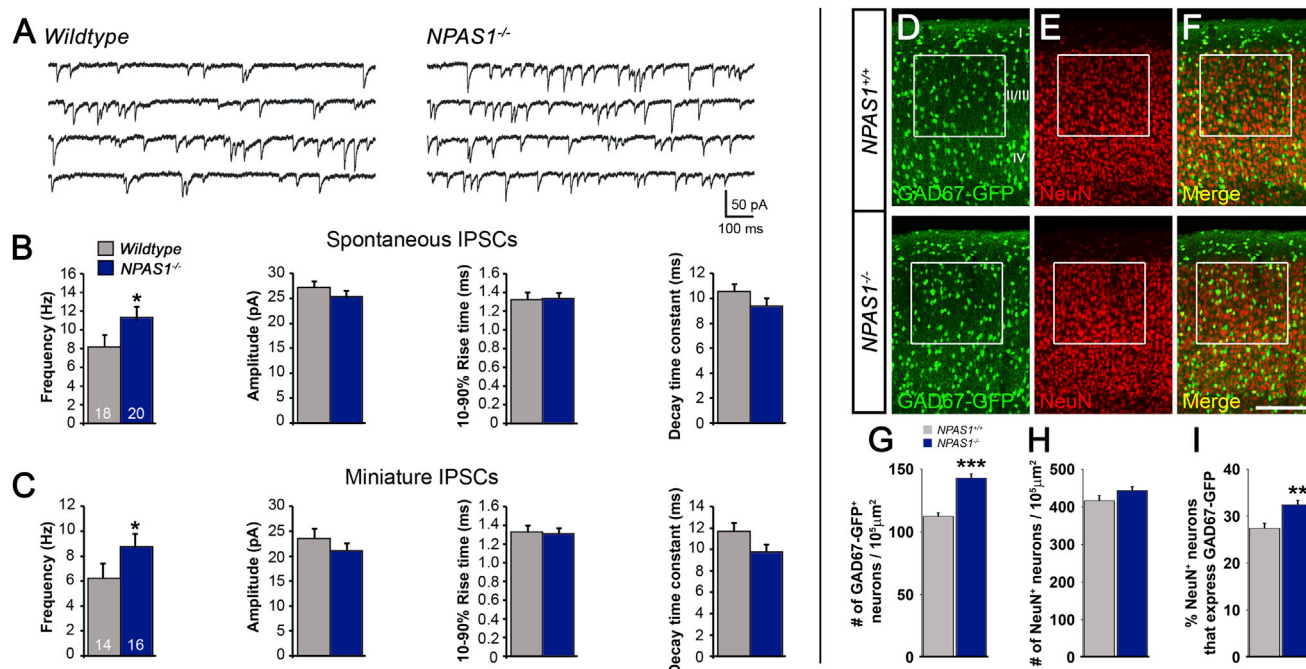


**Figure 4. Synaptic Inhibition to Neocortical Pyramidal Cells Is Increased in *NPAS1*<sup>-/-</sup> Mice**

(A) Representative traces of sIPSCs recorded from layer II/III pyramidal neurons in somatosensory neocortex of WT and *NPAS1*<sup>-/-</sup> mice. (B and C) Mean sIPSC (B) and mIPSC (C) frequencies were higher in pyramidal neurons recorded from *NPAS1*<sup>-/-</sup> mice than in controls. Numbers of recorded cells are shown in each bar. No significant changes in sIPSC or mIPSC amplitude, 10–90% rise time, or decay time constant were detected. For (B) and (C), *n* = 7 WT and 9 *NPAS1*<sup>-/-</sup> animals.

(D–F) Increase in GAD67-GFP<sup>+</sup> interneurons (D) and percentage of neurons (NeuN<sup>+</sup>) that are inhibitory (GAD67-GFP<sup>+</sup>) (F) within layer II/III of *NPAS1*<sup>-/-</sup> somatosensory cortex (white boxes) shown on coronal sections at P21. The density of NeuN<sup>+</sup> cells within layer II/III is not significantly increased in *NPAS1*<sup>-/-</sup> mutants (E).

(G–I) Quantification of GAD67-GFP<sup>+</sup> (G) and NeuN<sup>+</sup> (H) neurons/10<sup>5</sup> μm<sup>2</sup> and percentage of NeuN<sup>+</sup> cells that express GAD67-GFP within that area (I). *n* = 3 animals per genotype for (G)–(I). \**p* < 0.05. \*\**p* < 0.01. \*\*\**p* < 0.001. Scale bar, (D)–(F), 200 μm. See also Figure S4.

BrdU labeling analysis of E13.5 MGE and CGE progenitors, utilized to detect cells in S phase, supported the PH3 results. One hour BrdU pulse labeling showed increased proliferation in the SVZ of the *NPAS1*<sup>-/-</sup> mutant MGE (total number, 31% ± 1.26%, *p* = 0.0007; density, 48% ± 2.15%, *p* = 0.0004) and CGE (total number, 19% ± 3.31%, *p* = 0.039; density, 34% ± 5.24%, *p* = 0.022), while *NPAS3*<sup>-/-</sup> mutant mice exhibited decreased proliferation in the MGE SVZ (total number, 26% ± 2.05%, *p* = 0.0018; density, 21% ± 3.08%, *p* = 0.023) (Figures S5A–S5E). In addition, examination of proliferation in the hippocampal dentate gyrus following intraperitoneal injection of BrdU once daily for 12 days revealed a 31% increase (31% ± 7.89%, *p* = 0.003) in BrdU<sup>+</sup> cells in 5- to 10-week-old *NPAS1*<sup>-/-</sup> mice (Figures S5F and S5G).

The *NPAS Drosophila* homolog *Trachealess* regulates FGF signaling (Ohshiro and Saigo, 1997); thus we examined activation of the MAP kinase pathway by measuring the level of phospho-ERK immunofluorescence. *NPAS1* mutants had a 1.3-fold increase (E13.5 CGE, 1.32 ± 0.043, *p* = 0.0016; E15.5 MGE, 1.35 ± 0.063, *p* = 0.00017) in phospho-ERK expression in the E13.5 CGE and E15.5 MGE, whereas *NPAS3* mutants exhibited a 1.3-fold decrease (1.26 ± 0.060, *p* = 0.0079) in phospho-ERK expression in the E13.5 CGE and a 1.2-fold decrease (1.17 ±

0.024, *p* = 0.023) in the E13.5 MGE (Figures 5C, 5D, 5G, 5H, 5J, 5L, 5O, 5P, 5S, 5T, 5V, and 5X).

### ***NPAS1*<sup>-/-</sup> Ganglionic Eminences Displayed Increased *Arx* Expression which Mediated an Increase in Subpallial MAP Kinase Activity and Proliferation**

We focused on identifying molecular mechanisms underlying the increased proliferation and phospho-ERK expression in the MGE and CGE of *NPAS1* mutants by ISH screening of the MGE and CGE for expression of genes that are implicated in these processes (*Arx*, *COUP-TFI*, *Cyclin D1*, *Cyclin D2*, *Dlx1*, *ErbB4*, *FGFR1*, *FGFR3*, *Lhx2*, *Lhx6*, *NPAS3*, *Olig1*, *Sp8*, and *Sprouty2*) (Figures 6 and S5; data not shown). While we did not find robust changes for most of these, including FGF-signaling components, there were some interesting changes in *Arx* and *Sp8* expression. In accordance with the increase in CGE proliferation, there was a subtle increase in *Sp8*<sup>+</sup> (LGE/CGE marker) migrating interneurons at E13.5 (Figure 6B) (Ma et al., 2012). We also observed a clear increase of *Arx* TF RNA at E13.5 and E15.5 in regions of the MGE and CGE where *NPAS1* is normally expressed (Figures 6A and 6C). *Arx* function is necessary for proper interneuron migration and maturation (Colombo et al., 2007; Kitamura et al., 2002; Marsh et al., 2009), as well as neocortical neuron

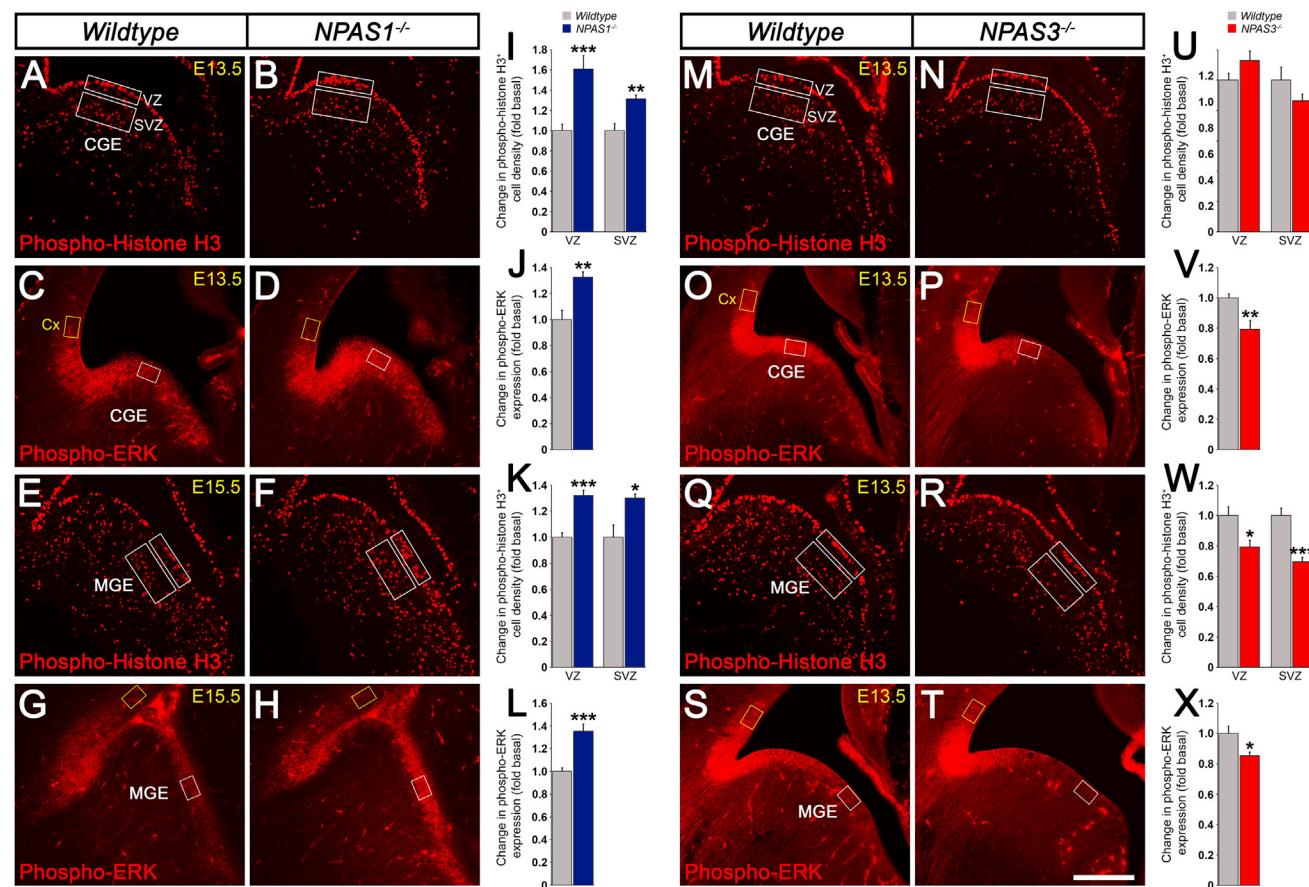


**Figure 5. NPAS1<sup>-/-</sup> Progenitors Have Increased Proliferation and MAP Kinase Activity, while NPAS3<sup>-/-</sup> Progenitors Exhibit Decreased Proliferation and MAP Kinase Activity**

(A–H) Immunofluorescence assays of coronal sections demonstrate increased proliferation (phosphohistone H3<sup>+</sup> M phase cells) and MAP kinase activity (phospho-ERK) in the E13.5 CGE (A–D), and E15.5 MGE (E–H) of NPAS1<sup>-/-</sup> progenitors.

(I–L) Quantification of phosphohistone H3<sup>+</sup> (I and K) cells and phospho-ERK (J and L) levels in NPAS1<sup>-/-</sup> mutants. n = 3 animals per genotype for (I)–(L).

(M–T) NPAS3<sup>-/-</sup> progenitors display reduced proliferation and MAP kinase activity in the E13.5 CGE (M–P). While MAP kinase activity was decreased in the E13.5 CGE (O and P), proliferation of progenitors was unaltered in the E13.5 CGE (M and N) of NPAS3<sup>-/-</sup> mutant mice.

(U–X) Quantification of phosphohistone H3<sup>+</sup> (U and W) cells and phospho-ERK (V and X) levels in NPAS3<sup>-/-</sup> mutants. Proliferation was measured in the VZ and SVZ (white boxes). Phospho-ERK levels in the CGE/MGE (white box) were normalized by comparison with cortical levels (yellow box). n = 3 animals per genotype for (U)–(X). Abbreviations are as follows: CGE, caudal ganglionic eminence; Cx, cortex; MGE, medial ganglionic eminence; SVZ, subventricular zone; VZ, ventricular zone. \*p < 0.05. \*\*p < 0.01. \*\*\*p < 0.001. Scale bar, (A)–(H) and (M)–(T), 250 μm. See also Figure S5.

progenitor proliferation (Friocourt et al., 2008; Kitamura et al., 2002).

To test whether NPAS1 and its cofactor, ARNT, can directly repress *Arx* expression through a known *Arx* subpallial enhancer element (Colasante et al., 2008; Visel et al., 2013), we performed luciferase assays in CGE primary cultures (Flandin et al., 2011). We found that this enhancer had two putative NPAS1/ARNT sites, designated A and B (Figure S7D) (Hogenesch et al., 1997). Consistent with the aforementioned phenotype, NPAS1/ARNT induced an ~2-fold repression of the *Arx* enhancer ( $0.58 \pm 0.035$ ,  $p = 6.69 \times 10^{-5}$ ). Mutation of the *Arx* enhancer at site A, but not site B, resulted in a rescue of the repression induced by NPAS1/ARNT ( $p = 0.034$ ) (Figures 7C and 7D).

Next, to investigate whether the increase in *Arx* expression (Figures 6A and 6C) could alter subpallial development, we used ultrasound to guide injection into the E13.5 CGE of a lenti-

virus encoding either *Arx* and GFP, or GFP alone. At E15.5, we compared the number of PH3<sup>+</sup>/GFP<sup>+</sup> cells and observed that the *Arx*-encoding virus increased PH3<sup>+</sup>/GFP<sup>+</sup> cells by ~2-fold ( $2.18 \pm 0.039$ ,  $p = 0.042$ ) (Figures 7A, 7B, and S7A). We also assessed the level of phospho-ERK expression in GFP<sup>+</sup> regions of the CGE ventricular zone and found that *Arx* overexpression increased phospho-ERK expression by 1.4-fold ( $1.39 \pm 0.12$ ,  $p = 0.046$ ) (Figures S7B and S7C). These findings provide evidence that NPAS1 repression of *Arx* can regulate CGE proliferation and MAP kinase activity.

### Nonsynonymous Mutations in NPAS1 and NPAS3 Are Found in Humans with ASD

NPAS3 mutations are observed in patients with schizophrenia (Kamnasaran et al., 2003; Macintyre et al., 2010). Given that ASDs and schizophrenia share some genetic risk factors

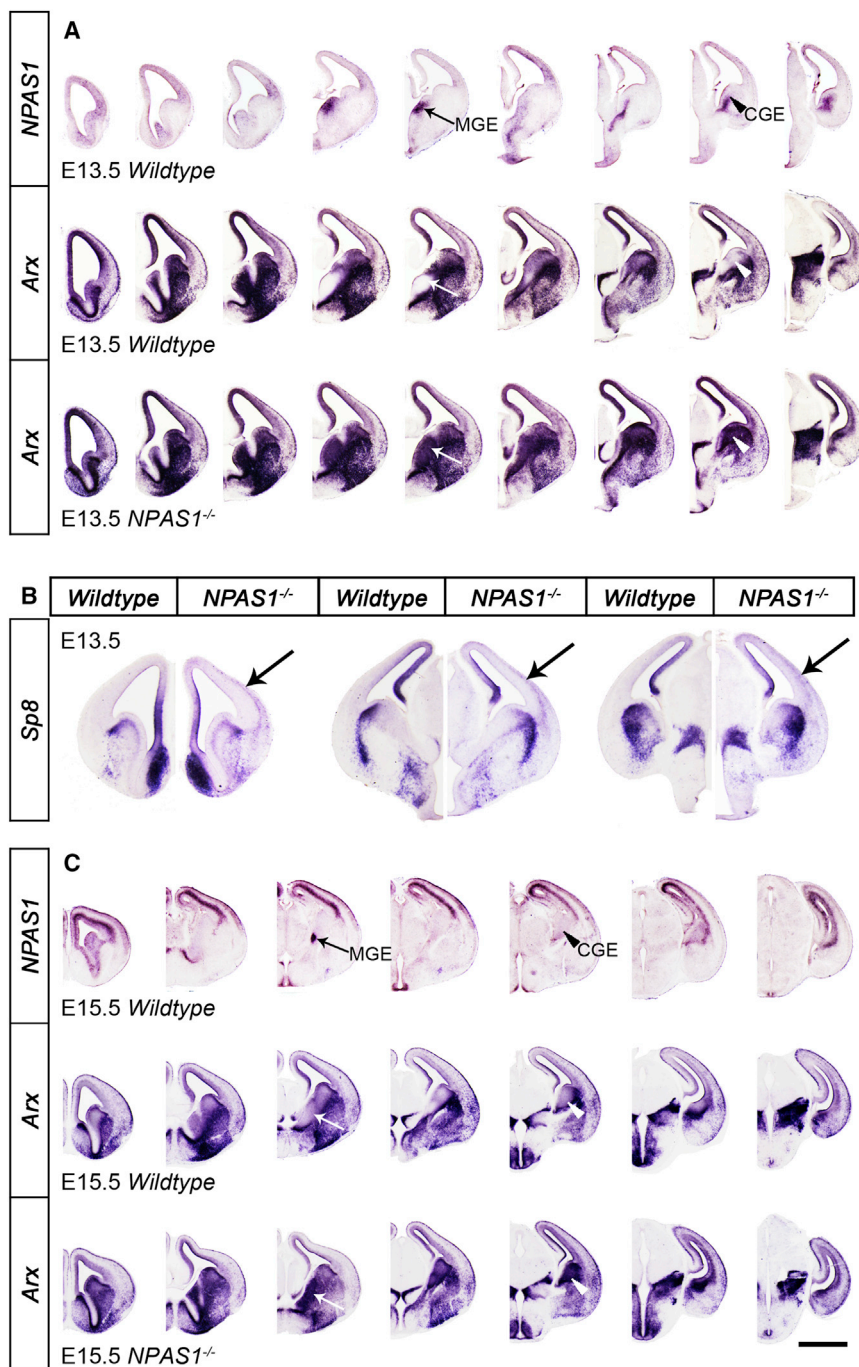


**Figure 6. NPAS1<sup>-/-</sup> GEs Have Increased Arx Expression, whereas NPAS1<sup>-/-</sup> Cortices Reveal Increased Sp8 Expression**

(A) ISH assay on coronal hemisections arrayed in a rostrocaudal series reveal that NPAS1<sup>-/-</sup> progenitors have increased Arx expression in the VZ/SVZ regions of the E13.5 MGE (arrows) and CGE (arrowheads) (compare white arrow and arrowhead in bottom tier [NPAS1<sup>-/-</sup>] to middle tier [WT]) where NPAS1 is expressed (black arrow and arrowhead in top tier).

(B) At E13.5, Sp8 expression appears increased in a pattern consistent with tangentially migrating cortical interneurons (arrows). Data are presented in coronal sections at three rostrocaudal planes (left to right).

(C) ISH assay on coronal hemisections displayed in a rostrocaudal series shows that NPAS1<sup>-/-</sup> progenitors have increased Arx expression in the VZ/SVZ regions of the E15.5 MGE (arrows) and CGE (arrowheads) (compare white arrow and arrowhead in bottom tier [NPAS1<sup>-/-</sup>] to middle tier [WT]) where NPAS1 is expressed (black arrow and arrowhead in top tier). Abbreviations are as follows: CGE, caudal ganglionic eminence; MGE, medial ganglionic eminence. Scale bar, (A) 1 mm, (B) 723  $\mu$ m, and (C) 1.25 mm. See also Figure S6.

tistical power and do not unambiguously implicate these variants in genetic susceptibility to ASD, these results support the possibility that NPAS1 and NPAS3 mutations are related to ASD risk.

## DISCUSSION

NPAS1<sup>-/-</sup> mice had increased numbers of neocortical interneurons, whereas NPAS3<sup>-/-</sup> mice have fewer interneurons (Figures 3A–3C, 3E, 3A'–3C', 3E', 3A''–3C'', 3E'', 3F–3H, and 3J). These changes in interneuron numbers were associated with altered ERK signaling and cell proliferation within the MGE and CGE of NPAS1<sup>-/-</sup> and NPAS3<sup>-/-</sup> mutants (Figure 5). In addition, the increased numbers of neocortical interneurons in NPAS1<sup>-/-</sup> mice resulted in enhanced synaptic inhibition onto neocortical pyramidal neurons in layer II/III of the somatosensory cortex

(Murdoch and State, 2013) and, like NPAS1 mutant mice, enlarged brain size is frequent in ASD children (Butler et al., 2005; Hazlett et al., 2011), we screened 947 ASD probands for mutations in NPAS1 and NPAS3 exons, introns, and 5' and 3' untranslated regions, and found ten nonsynonymous variants in NPAS1 and seven in NPAS3 (see the Supplemental Information). We assayed 13 of those in 190 control subjects (unscreened for autism) and found that five of seven in NPAS1 and all six in NPAS3 were absent in the controls. Although the data lack sta-

(Figures 4A–4C). We focused on how NPAS1 regulates this process in the MGE and CGE and found that NPAS1<sup>-/-</sup> mutants had increased Arx expression in these embryonic progenitor zones (Figures 6A and 6C). Using in utero transduction of Arx into the CGE, we showed that increased Arx expression was sufficient to increase subpallial proliferation and MAP kinase activity (Figures 7A, 7B, S7B, and S7C). We also demonstrated that NPAS1 could directly repress a bone fide Arx subpallial enhancer (Figures 7C, 7D, and S7D) (Colasante et al., 2008).

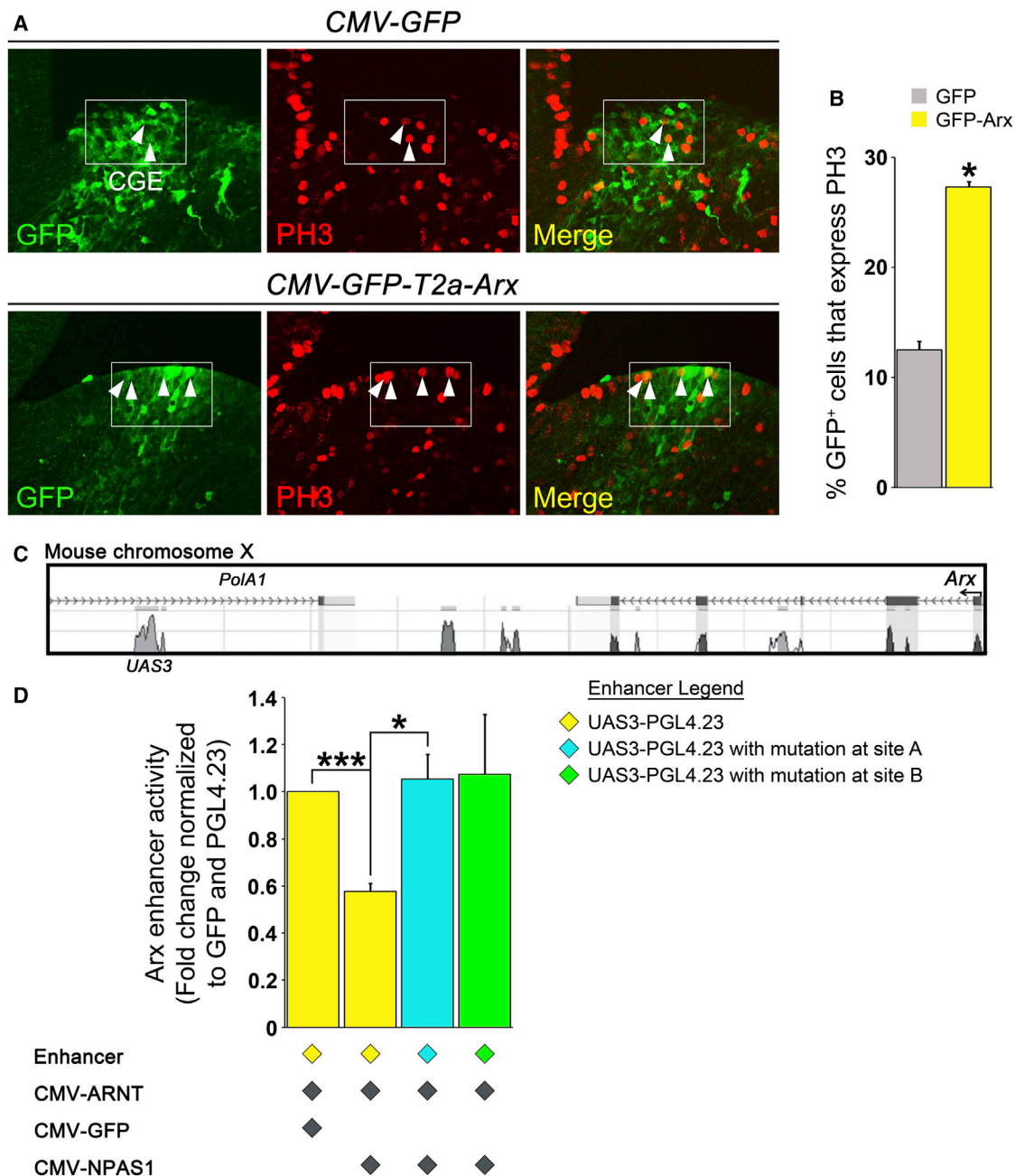


**Figure 7. Increased *Arx* Expression in the CGE Mediates Increased Subpallial Proliferation**

(A and B) In utero lentiviral transduction of *Arx* into the E13.5 CGE results in increased cell proliferation (PH3). Arrowheads in (A) indicate GFP<sup>+</sup>/PH3<sup>+</sup> cells. n = 3 animals per experimental condition for (B).

(C) *Arx* locus on mouse X chr, showing evolutionarily conserved domains, one of which is a subpallial enhancer (UAS3) (Colasante et al., 2008; Visel et al., 2013) that has two predicted NPAS1/ARNT sites (Figure S6).

(D) Transcription assay of E12.5 CGE primary culture shows that NPAS1/ARNT expression represses activity of the *Arx* subpallial enhancer. Mutation of the *Arx* enhancer at site A, but not site B, resulted in a rescue of the repression induced by NPAS1/ARNT. n = 3 independent experiments, each performed in triplicate for (D). Abbreviations are as follows: CGE, caudal ganglionic eminence. \*p < 0.05. \*\*p < 0.01. Scale bar, (A) 70 μm. See also Figure S7.

Our results provide insights into mechanisms that control the number of specific subtypes of cortical inhibitory neurons, showing that homologous TF-encoding genes NPAS1 and

NPAS3 have opposing functions in regulating the numbers of SST<sup>+</sup> and VIP<sup>+</sup> interneurons (Figures 3A–3A', 3E–3E'', 3F, and 3J). Thus, we have provided evidence for a cell-autonomous

mechanism that controls interneuron numbers, a process proposed to exist based on results from the MGE-transplantation assay (Southwell et al., 2012).

### NPAS1 and NPAS3 Regulate the Proliferation of Ganglionic Eminence Progenitors

Proliferation and ERK signaling in progenitor domains of the MGE and CGE were increased and decreased in *NPAS1*<sup>-/-</sup> and *NPAS3*<sup>-/-</sup> mice, respectively (Figure 5). Vertebrate NPAS function in embryonic neural precursors may be related to the function of *Trachealess*, the NPAS *Drosophila* homolog. *Trachealess* promotes FGF-signaling by increasing expression of the FGF receptor (Ohshiro and Saigo, 1997). This program is evolutionarily conserved based on the observation that *NPAS3*<sup>-/-</sup> mice have reduced *FGFR1* expression in the adult hippocampus (Pieper et al., 2005). However, *NPAS3*<sup>-/-</sup> mutant mice did not show this phenotype in the prenatal telencephalon (data not shown). Also, *NPAS1*<sup>-/-</sup> mutants did not exhibit decreased *FGFR1* expression in the adult hippocampus (Pieper et al., 2005), or in the prenatal telencephalon (Figure S6C). Thus, there is no evidence that changes in phospho-ERK levels, in the subpallium of *NPAS1*<sup>-/-</sup> and *NPAS3*<sup>-/-</sup> mutants (Figures 5C, 5D, 5G, 5H, 5J, 5L, 5O, 5P, 5S, 5T, 5V, and 5X), are related to altered FGF signaling.

Our study reveals insights into NPAS1 regulation of cell proliferation. Here, we have found that the increase in proliferation and MAPK signaling in *NPAS1*<sup>-/-</sup> mutant CGE and MGE progenitors was associated with increased *Arx* expression. Previous studies of *Arx* mutant mice show that lack of this TF resulted in reduced cortical proliferation (Friocourt et al., 2008; Kitamura et al., 2002). We demonstrated that increased *Arx* expression was sufficient to enhance subpallial proliferation and MAP kinase activity, using in utero transduction of *Arx* into the CGE (Figures 7A, 7B, S7B, and S7C). Furthermore, we showed that NPAS1 could directly inhibit a bone fide *Arx* subpallial enhancer (Figures 7C, 7D, and S7D) (Colasante et al., 2008).

Given that NPAS1 and NPAS3 have opposite effects on proliferation, an imbalance of either NPAS1 or NPAS3 expression and/or function could potentially be compensated by changes in the expression of the other gene. However, we did not observe changes of NPAS3 expression in the *NPAS1*<sup>-/-</sup> E13.5 and P0 forebrain (data not shown).

### NPAS1 and NPAS3 Modified the Production of Specific Subtypes of Cortical Interneurons

The increase in *Arx* and phospho-ERK expression and the increase in proliferation in the MGE and CGE of *NPAS1*<sup>-/-</sup> mutants were associated with an increase in subpallially derived cortical interneurons (Figure 2). As a result, NPAS1 mutants had excessive SST<sup>+</sup> and VIP<sup>+</sup> interneurons, products of the MGE and CGE, respectively (Figures 3A, 3A', 3E, 3E', 3F, and 3J) (Rudy et al., 2011). In contrast, decreased phospho-ERK expression and cell proliferation in the MGE and CGE of *NPAS3*<sup>-/-</sup> mutant mice resulted in reduced numbers of SST<sup>+</sup> and VIP<sup>+</sup> interneurons (Figures 3A, 3A', 3E, 3E', 3F, and 3J).

Both NPAS1 and NPAS3 mutants had a normal density of PV<sup>+</sup> interneurons (Figures 3D–3D' and 3I). PV and SST are MGE derived (Rudy et al., 2011). NPAS1, along with NPAS3, COUP-

*TFI*, *Dlx1*, and *SatB1* (Cobos et al., 2005; Denaxa et al., 2012; Lodata et al., 2011), define a set of TFs that differentially regulate the numbers of interneurons that express PV and SST (Figures 3D–3D', 3E–3E', 3I, and 3J). At least one PV<sup>+</sup> subtype, the Chandelier neuron, is generated late in gestation (Inan et al., 2012; Taniguchi et al., 2013); perhaps NPAS1 and NPAS3 regulation of MGE proliferation is time dependent, and thus preferentially affects early-born SST<sup>+</sup> interneurons. Based on the embryonic phenotypes of *NPAS1*<sup>-/-</sup> and *NPAS3*<sup>-/-</sup> mutants, we propose that NPAS1 and NPAS3 control the SST/PV ratio via their functions in MGE progenitor cells. Future studies are needed to examine the roles of NPAS1 and NPAS3 in regulating interneurons via their expression in maturing and mature interneurons (Figure 1C).

The significance of transcriptional repression in the regulation of cortical interneuron number is becoming apparent. A recent study demonstrates that Olig1 inhibits the generation of GABAergic interneurons produced in the MGE by repression of *Dlx* expression through the *Dlx1/2/12b* intergenic enhancer (Silbereis et al., 2014). Likewise, NPAS1 inhibits the generation of cortical interneurons by repression of *Arx* expression through the subpallial *Arx* enhancer, which mediates CGE progenitor cell proliferation (Figure 7) (Colasante et al., 2008).

### NPAS1 Function in Interneuron Generation Controls Cortical Excitation/Inhibition

*NPAS1*<sup>-/-</sup> mutant mice display increased numbers of GAD67-GFP<sup>+</sup> interneurons in layer I (Figure S4C). It is likely that an excess of GABAergic neurons in layer I would have an effect on the inhibitory tone of pyramidal cell dendrites within this layer. NPAS1 mutants also exhibit excessive SST<sup>+</sup> and VIP<sup>+</sup> interneurons. VIP<sup>+</sup> interneurons are enriched in layers II/III (Kawaguchi and Kubota, 1997; Miyoshi et al., 2010) and form synapses with pyramidal cell somata and dendrites (Kawaguchi and Kubota, 1996) and other interneurons (Acsády et al., 1996; Dávid et al., 2007; Hajos et al., 1996). Thus, with an increase in both SST<sup>+</sup> and VIP<sup>+</sup> interneurons, it is difficult to deduce the net physiological effect a priori. We found that NPAS1 mutants had enhanced cortical inhibition in layer II/III of the somatosensory cortex (Figure 4), implying that the increase in interneurons resulted in a net increase in inhibition in superficial cortical layers. The enhanced cortical inhibition in layer II/III somatosensory cortex of *NPAS1*<sup>-/-</sup> mutants suggests a decreased E/I ratio in layer II/III somatosensory cortex. This is supported by estimation of the cellular E/I ratio within this cortical region of *NPAS1*<sup>-/-</sup> mutant mice (Figure S4D). While increased cortical inhibition is likely to reduce noise in the cortex, and it could be protective for epilepsy, it may be detrimental to cortical function by dampening cortical signals and thereby predispose to neuropsychiatric disorders.

### NPAS1 and NPAS3 in Human Neuropsychiatric Disorders

Our examination of NPAS1 and NPAS3 functions in mice provides mechanistic insights into human neuropsychiatric disorders. NPAS3<sup>-/-</sup> mutant mice display behavioral and neuroanatomical deficits associated with human schizophrenia (Erbel-Sieler et al., 2004), and NPAS3 mutations are observed in

patients with schizophrenia (Kamnasaran et al., 2003; Macintyre et al., 2010). Furthermore, *NPAS1* mutant mice exhibit an increase in brain size (Figures S3D–S3G), similar to the enlargement seen in some children with ASD (Butler et al., 2005; Hazlett et al., 2011). Notably, we have found sporadic nonsynonymous mutations in *NPAS1* and *NPAS3* in individuals with ASD, which suggests that *NPAS1* and *NPAS3* mutations may be associated with ASD risk. However, our analyses lack the statistical power to conclude that these alleles contribute to ASD. Nonetheless, these data, and the experimental analyses of the mouse mutants, strongly suggest that further genetic analyses of *NPAS1* and *NPAS3* are warranted in human neuropsychiatric disorders.

## EXPERIMENTAL PROCEDURES

### Mice

*NPAS1*<sup>+/-</sup> and *NPAS3*<sup>+/-</sup> mice were obtained from Steven McKnight (University of Texas Southwestern Medical Center) and genotyped as described by Erbel-Sieler and colleagues (Erbel-Sieler et al., 2004). *NPAS1*<sup>+/-</sup> mice were maintained in a C57BL/6J strain background. *NPAS1*<sup>+/-</sup>; *NPAS3*<sup>+/-</sup> females mated to *NPAS1*<sup>+/-</sup>; *NPAS3*<sup>+/-</sup> males also produced C57BL/6J strain litters. *NPAS3*<sup>-/-</sup> mutant mice obtained from this cross were utilized for BrdU analysis of the ganglionic eminences, assessment of cortical layer-specific markers, and in the examination of interneuron markers in the P30 somatosensory cortex. However, due to increased mortality of *NPAS3*<sup>-/-</sup> mutants maintained on a C57BL/6J strain background, subsequent experiments were performed with *NPAS3*<sup>-/-</sup> mutant mice maintained on a CD-1 strain background. These experiments include assessment of apoptosis within the somatosensory cortex, examination of PH3 and phospho-ERK expression in the ganglionic eminences, and MRI analysis.

The *Lhx6-GFP* BAC transgenic mouse line was obtained from the Gene Expression Nervous System Atlas Project (GENSAT) at The Rockefeller University (New York). *GAD67-GFP* mice were genotyped as described by Tamamaki and colleagues (Tamamaki et al., 2003). As a note on nomenclature, experimental samples designated as *NPAS1*<sup>+/-</sup> indicate that the *NPAS1* allele is unaltered; however, data from these mice are not referred to as WT because they have either the *Lhx6-GFP* or *GAD67-GFP* alleles. CD-1 WT mice were obtained from Charles River Laboratories. WT littermate mice were used as controls for all experiments. For staging of embryos, midday of the vaginal plug was calculated as embryonic day 0.5 (E0.5). Mouse colonies were maintained at the University of California, San Francisco, and University of Texas Southwestern Medical Center, in accordance with National Institutes of Health, UCSF, and UT Southwestern guidelines.

### Histology

See the [Supplemental Experimental Procedures](#) for details on immunohistochemistry, ISH, BrdU labeling, and Nissl stain analysis.

### MRI

P30 4% PFA-fixed brains were washed twice in 20 ml PBS for a total of 24 hr and imaged in Fluorinert FC-40 (Sigma Aldrich) for null background signal. The imaging was done on a 600 MHz NMR spectrometer (Agilent Technologies Inc.) with imaging gradients and the following parameters: 3D gradient echo, TE/TR 15/75 ms, eight averages, field of view (FOV) 12.8 mm isotropic, resolution of 50  $\mu$ m  $\times$  50  $\mu$ m  $\times$  100  $\mu$ m, and a total scan time of 5.5 hr. The acquired images were converted on the Varian console to the DICOM format and reformatted into the same orientation as the histology sections using OsiriX, an open source image viewer. Volumetric measurements were made using custom-built software in MATLAB. Cortical and basal ganglia volumes were statistically analyzed in three mice of each genotype. Results are presented as mean  $\pm$  SEM. Statistical differences between experimental groups were assessed with the Student's *t* test using SPSS 15 software (IBM). See [Table S3](#) in the [Supplemental Experimental Procedures](#) for details on cortical and basal ganglia volumes in control, *NPAS1*<sup>-/-</sup>, and *NPAS3*<sup>-/-</sup> mutants.

### Electrophysiology

Coronal brain slices (300  $\mu$ m) were prepared from P21–30 WT and *NPAS1*<sup>-/-</sup> mice. Slices were submerged in the recording chamber and continuously perfused with oxygenated ACSF (32–34°C) containing (in mM) 124 NaCl, 3 KCl, 1.25 NaH<sub>2</sub>PO<sub>4</sub>·H<sub>2</sub>O, 2 MgSO<sub>4</sub>·7H<sub>2</sub>O, 26 NaHCO<sub>3</sub>, 10 dextrose, and 2 CaCl<sub>2</sub> (pH 7.2–7.4, 300–305 mOsm/kg). Whole-cell patch-clamp recordings from layer II/III pyramidal cells in somatosensory neocortex were performed at 40 $\times$  using an upright, fixed-stage microscope (Olympus BX50WI) equipped with infrared, differential interference contrast (IR-DIC). Patch pipettes (2–4 M $\Omega$ ) were filled with an internal solution, containing (in mM) 140 CsCl, 1 MgCl<sub>2</sub>, 10 HEPES, 11 EGTA, 2 NaATP, 0.5 Na<sub>2</sub>GTP, and 1.25 QX-314 (pH 7.28). Recordings were obtained with an Axopatch 1D amplifier, filtered at 5 kHz, and recorded to pClamp 10.2 software (Clampfit, Axon Instruments). Spontaneous (s) and miniature (m) IPSCs were examined at a holding potential of  $-70$  mV. GABAergic currents were isolated by adding 1 mM kynurenic acid to the ACSF to block glutamate receptors, and tetrodotoxin (TTX, 2  $\mu$ M) was added to isolate mIPSCs. Series resistance was typically <15 M $\Omega$  and was monitored throughout the recordings. Data were only used for analysis if the series resistance remained <20 M $\Omega$  and changed by  $\leq 20\%$  during the recordings. Data analysis was performed using pClamp 10.2 (Clampfit, Axon Instruments), MiniAnalysis 6.0 (Synaptosoft), Microsoft Excel, and SigmaPlot 12.3 programs. Events characterized by a typical fast rising phase and exponential decay phase were manually detected using MiniAnalysis. A 2 min sample recording per cell was used for measuring IPSC frequency, amplitude, 10%–90% rise time, and decay time constant. Kinetic analysis of the IPSCs was performed with a single-exponential function. The threshold for event detection was currents with amplitudes greater than three times the root mean square (rms) noise level. Spontaneous IPSC measurements were recorded from 18 wild-type and 20 *NPAS1*<sup>-/-</sup> pyramidal cells. Miniature IPSC measurements were recorded from 14 WT and 16 *NPAS1*<sup>-/-</sup> pyramidal cells. Seven WT and nine *NPAS1*<sup>-/-</sup> animals were used for sIPSC and mIPSC measurements. Results are expressed as mean  $\pm$  SEM. Statistical differences between experimental groups were assessed with the Mann-Whitney *U* test using SigmaPlot 12.3 software (SYSTAT).

### Primary Cell Culture and Luciferase Assays

CGE tissue was dissected from E12.5 WT embryos and mechanically dissociated with a P1000 pipette tip. A total of 200,000 cells were seeded into tissue culture dishes precoated with poly-L-lysine 10  $\mu$ g/ml (Sigma) and then laminin (5  $\mu$ g/ml, Sigma), and grown in N5 media (DMEM-F-12 with glutamax, N2 supplement, 35  $\mu$ g/ml bovine pituitary extract, 20 ng/ml bFGF, and 20 ng/ml EGF) as previously described for MGE cells (Flandin et al., 2011).

CGE primary cultures were transfected using Eugene 6 (Promega) with DNA expression vectors and reporters comprising four conditions: (1) empty firefly-luciferase reporter (PGL4.23) and a control DNA expression vector only expressing GFP (CMV-GFP), (2) empty PGL4.23 and CMV-NPAS1, (3) Arx enhancer (UAS3-PGL4.23) luciferase reporter and CMV-GFP, and (4) UAS3-PGL4.23 and CMV-NPAS1. All conditions also included the same amounts of CMV-ARNT (NPAS cofactor) and Renilla-luciferase (normalization control). Cell lysates were collected at 2 days posttransfection and procedures were performed according to the manufacturer's protocol (Promega, dual luciferase assay system). Enhancer activity for each condition was determined from three independent experiments, each performed in triplicate. Results were calculated as mean  $\pm$  SEM and presented as fold change relative to the basal condition containing CMV-GFP and the PGL4.23 empty luciferase reporter vector. Statistical differences between experimental groups were determined with the Student's *t* test using SPSS 15 software (IBM). See the [Supplemental Experimental Procedures](#) for details on expression and luciferase reporter vectors.

### Virus Production and In Utero Injection

HEK293T cells grown in DMEM H21 with 10% FBS were transfected with four plasmids to generate lentivirus particles, (pVSV-g, pRSVr, pMDLg-pRRE, and the lentiviral vector). Cells were transfected at  $\sim 70\%$  confluency, and media was completely replaced 4 hr after transfection, then cultured for 4 days before harvesting. On day 4 of culture, all the media ( $\sim 35$  ml) was

collected and filtered through a 0.45 low protein binding membrane to remove cells and large debris. The filtered media was pooled and ultracentrifuged at  $100,000 \times g$  for 2.5 hr at  $4^{\circ}\text{C}$ . After the ultracentrifuge step, supernatant was removed, and the pellet was resuspended overnight in sterile PBS, then stored at  $-80^{\circ}\text{C}$  until use. For infection, recipient pregnant females (E13.5) were anesthetized with isoflurane, their uterine horns exposed, and mounted under an ultrasound microscope (Vevo 770, VisualSonics). A beveled glass micropipette ( $\sim 50 \mu\text{m}$  diameter) was front loaded with CMV-GFP or CMV-GFP-T2a-Arx lentivirus and inserted into the VZ of the CGE under real-time ultrasound guidance imaging. Approximately  $1 \mu\text{l}$  of solution was injected into the VZ of the CGE. Three successfully injected animals were analyzed 2 days later (E15.5) for each experimental condition. Image analysis of CMV-GFP<sup>+</sup>/PH3<sup>+</sup>, CMV-GFP<sup>+</sup>/phospho-ERK<sup>+</sup>, CMV-GFP-T2a-Arx<sup>+</sup>/PH3<sup>+</sup>, or CMV-GFP-T2a-Arx<sup>+</sup>/phospho-ERK<sup>+</sup> coexpression was performed on images acquired on a confocal microscope (LSM 510 META NLO, Carl Zeiss International) with a  $20\times$  objective. The percentage of CMV-GFP<sup>+</sup> or CMV-GFP-T2a-Arx<sup>+</sup> that expresses PH3 was calculated in a  $10,000 \mu\text{m}^2$  area of the CGE VZ. Results are presented as mean  $\pm$  SEM. Statistical differences between experimental groups were assessed with the chi-square test using SPSS 15 software (IBM). Phospho-ERK expression levels were measured in GFP<sup>+</sup> regions of the CGE VZ with the aid of Adobe Photoshop CS4 software. Expression levels were determined as a ratio of the integrated density of phospho-ERK<sup>+</sup> CGE VZ cells in a  $4,000 \mu\text{m}^2$  area to the integrated density of phospho-ERK<sup>+</sup> cortical VZ cells in a  $4,000 \mu\text{m}^2$  area. Integrated density is equal to the sum of the pixel values in a selected area. Results were calculated as mean  $\pm$  SEM and presented as fold change relative to control. Statistical differences between experimental groups were determined with the Student's *t* test using SPSS 15 software (IBM). See the [Supplemental Experimental Procedures](#) for details on lentiviral vectors.

#### Human DNA Sequencing

See the [Supplemental Experimental Procedures](#) for details on human DNA sequencing.

#### SUPPLEMENTAL INFORMATION

Supplemental Information includes seven figures, seven tables, Supplemental Experimental Procedures, and Supplemental Text and can be found with this article online at <http://dx.doi.org/10.1016/j.neuron.2014.10.040>.

#### ACKNOWLEDGMENTS

We are grateful to S. McKnight and his lab at University of Texas Southwestern Medical Center for the generous gift of NPAS1 and NPAS3 antibodies, the NPAS1<sup>+/−</sup> and NPAS3<sup>+/−</sup> mice, the NPAS1 ISH construct (J. Walker), and the CMV-ARNT and CMV-NPAS1 mammalian expression vectors (L. Wu). We acknowledge the Autism Genetic Resource Exchange (AGRE) and Simons Foundation Autism Research Initiative (SFARI) for ASD genomic DNA samples, and SFARI as well for phenotypic data made available on SFARI Base. We also wish to thank all the families who donated samples, and the principal investigators involved in their collection (A. Beaudet, R. Bernier, J. Constantino, E. Cook, E. Fombonne, D. Geschwind, D. Grice, A. Klin, D. Ledbetter, C. Lord, C. Martin, D. Martin, R. Maxim, J. Miles, O. Ousley, B. Peterson, J. Piggot, C. Saulnier, M. State, W. Stone, J. Sutcliffe, C. Walsh, and E. Wijsman). Approved researchers can obtain the Simons Simplex Collection (SSC) population data set by applying at <https://base.sfari.org>. This work was supported by research grants to J.L.R.R. (Simons Foundation, Nina Ireland, Althea Foundation, NIMH R37 MH049428, Weston Havens Foundation), to A.S. (NIMH T32 MH089920), to S.C.B. (R01NS071785), to R.F.H. (F32NS077747), to D.X. (R01EB009756), to S.P.H. (Jaffe Family Foundation), and to A.A.P. and Steven L. McKnight (NIMH 5-RO1-MH087986). This work was also funded in part by an unrestricted endowment provided to Steven L. McKnight by an anonymous donor, used as support for J.W.

Accepted: October 2, 2014

Published: November 20, 2014

#### REFERENCES

- Acsády, L., Arabadzisz, D., and Freund, T.F. (1996). Correlated morphological and neurochemical features identify different subsets of vasoactive intestinal polypeptide-immunoreactive interneurons in rat hippocampus. *Neuroscience* 73, 299–315.
- Azim, E., Jabaudon, D., Fame, R.M., and Macklis, J.D. (2009). SOX6 controls dorsal progenitor identity and interneuron diversity during neocortical development. *Nat. Neurosci.* 12, 1238–1247.
- Batista-Brito, R., Machold, R., Klein, C., and Fishell, G. (2008). Gene expression in cortical interneuron precursors is prescient of their mature function. *Cereb. Cortex* 18, 2306–2317.
- Batista-Brito, R., Rossignol, E., Hjerling-Leffler, J., Denaxa, M., Wegner, M., Lefebvre, V., Pachnis, V., and Fishell, G. (2009). The cell-intrinsic requirement of Sox6 for cortical interneuron development. *Neuron* 63, 466–481.
- Butler, M.G., Dasouki, M.J., Zhou, X.P., Talebizadeh, Z., Brown, M., Takahashi, T.N., Miles, J.H., Wang, C.H., Stratton, R., Pilarski, R., and Eng, C. (2005). Subset of individuals with autism spectrum disorders and extreme macrocephaly associated with germline PTEN tumour suppressor gene mutations. *J. Med. Genet.* 42, 318–321.
- Cobos, I., Calcagnotto, M.E., Vilaythong, A.J., Thwin, M.T., Noebels, J.L., Baraban, S.C., and Rubenstein, J.L.R. (2005). Mice lacking Dlx1 show subtype-specific loss of interneurons, reduced inhibition and epilepsy. *Nat. Neurosci.* 8, 1059–1068.
- Colasante, G., Collombat, P., Raimondi, V., Bonanomi, D., Ferrai, C., Maira, M., Yoshikawa, K., Mansouri, A., Valtorta, F., Rubenstein, J.L., and Broccoli, V. (2008). Arx is a direct target of Dlx2 and thereby contributes to the tangential migration of GABAergic interneurons. *J. Neurosci.* 28, 10674–10686.
- Colombo, E., Collombat, P., Colasante, G., Bianchi, M., Long, J., Mansouri, A., Rubenstein, J.L., and Broccoli, V. (2007). Inactivation of Arx, the murine ortholog of the X-linked lissencephaly with ambiguous genitalia gene, leads to severe disorganization of the ventral telencephalon with impaired neuronal migration and differentiation. *J. Neurosci.* 27, 4786–4798.
- Courchesne, E., Pierce, K., Schumann, C.M., Redcay, E., Buckwalter, J.A., Kennedy, D.P., and Morgan, J. (2007). Mapping early brain development in autism. *Neuron* 56, 399–413.
- Dávid, C., Schleicher, A., Zuschratter, W., and Staiger, J.F. (2007). The innervation of parvalbumin-containing interneurons by VIP-immunopositive interneurons in the primary somatosensory cortex of the adult rat. *Eur. J. Neurosci.* 25, 2329–2340.
- Denaxa, M., Kalaitzidou, M., Garefalaki, A., Achimastou, A., Lasrado, R., Maes, T., and Pachnis, V. (2012). Maturation-promoting activity of SATB1 in MGE-derived cortical interneurons. *Cell Rep.* 2, 1351–1362.
- Erbel-Sieler, C., Dudley, C., Zhou, Y., Wu, X., Estill, S.J., Han, T., Diaz-Arrastia, R., Brunskill, E.W., Potter, S.S., and McKnight, S.L. (2004). Behavioral and regulatory abnormalities in mice deficient in the NPAS1 and NPAS3 transcription factors. *Proc. Natl. Acad. Sci. USA* 101, 13648–13653.
- Flandin, P., Kimura, S., and Rubenstein, J.L. (2010). The progenitor zone of the ventral medial ganglionic eminence requires Nkx2-1 to generate most of the globus pallidus but few neocortical interneurons. *J. Neurosci.* 30, 2812–2823.
- Flandin, P., Zhao, Y., Vogt, D., Jeong, J., Long, J., Potter, G., Westphal, H., and Rubenstein, J.L. (2011). Lhx6 and Lhx8 coordinately induce neuronal expression of Shh that controls the generation of interneuron progenitors. *Neuron* 70, 939–950.
- Friocourt, G., Kanatani, S., Tabata, H., Yozu, M., Takahashi, T., Antypa, M., Raguénès, O., Chelly, J., Férec, C., Nakajima, K., and Parnavelas, J.G. (2008). Cell-autonomous roles of ARX in cell proliferation and neuronal migration during corticogenesis. *J. Neurosci.* 28, 5794–5805.
- Gelman, D.M., Marin, O., and Rubenstein, J.L.R. (2012). The generation of cortical interneurons. In *Jasper's Basic Mechanisms of the Epilepsies*, J.L. Noebels, M. Avoli, M.A. Rogawski, R.W. Olsen, and A.V. Delgado-Escueta, eds. (Bethesda, MD: National Center for Biotechnology Information).

- Gripp, K.W., Zand, D.J., Demmer, L., Anderson, C.E., Dobyns, W.B., Zackai, E.H., Denenberg, E., Jenny, K., Stabley, D.L., and Sol-Church, K. (2013). Expanding the SHOC2 mutation associated phenotype of Noonan syndrome with loose anagen hair: structural brain anomalies and myelofibrosis. *Am. J. Med. Genet. A* 161A, 2420–2430.
- Hajos, N., Acsady, L., and Freund, T.F. (1996). Target selectivity and neurochemical characteristics of VIP-immunoreactive interneurons in the rat dentate gyrus. *Eur. J. Neurosci.* 8, 1415–1431.
- Hazlett, H.C., Poe, M.D., Gerig, G., Styner, M., Chappell, C., Smith, R.G., Vachet, C., and Piven, J. (2011). Early brain overgrowth in autism associated with an increase in cortical surface area before age 2 years. *Arch. Gen. Psychiatry* 68, 467–476.
- Hogenesch, J.B., Chan, W.K., Jackiw, V.H., Brown, R.C., Gu, Y.Z., Pray-Grant, M., Perdew, G.H., and Bradfield, C.A. (1997). Characterization of a subset of the basic-helix-loop-helix-PAS superfamily that interacts with components of the dioxin signaling pathway. *J. Biol. Chem.* 272, 8581–8593.
- Inan, M., Welagen, J., and Anderson, S.A. (2012). Spatial and temporal bias in the mitotic origins of somatostatin- and parvalbumin-expressing interneuron subgroups and the chandelier subtype in the medial ganglionic eminence. *Cereb. Cortex* 22, 820–827.
- Kamnasaran, D., Muir, W.J., Ferguson-Smith, M.A., and Cox, D.W. (2003). Disruption of the neuronal PAS3 gene in a family affected with schizophrenia. *J. Med. Genet.* 40, 325–332.
- Kawaguchi, Y., and Kubota, Y. (1996). Physiological and morphological identification of somatostatin- or vasoactive intestinal polypeptide-containing cells among GABAergic cell subtypes in rat frontal cortex. *J. Neurosci.* 16, 2701–2715.
- Kawaguchi, Y., and Kubota, Y. (1997). GABAergic cell subtypes and their synaptic connections in rat frontal cortex. *Cereb. Cortex* 7, 476–486.
- Kitamura, K., Yanazawa, M., Sugiyama, N., Miura, H., Iizuka-Kogo, A., Kusaka, M., Omichi, K., Suzuki, R., Kato-Fukui, Y., Kamiyama, K., et al. (2002). Mutation of ARX causes abnormal development of forebrain and testes in mice and X-linked lissencephaly with abnormal genitalia in humans. *Nat. Genet.* 32, 359–369.
- Kwan, K.Y., Sestan, N., and Anton, E.S. (2012). Transcriptional co-regulation of neuronal migration and laminar identity in the neocortex. *Development* 139, 1535–1546.
- Le Magueresse, C., and Monyer, H. (2013). GABAergic interneurons shape the functional maturation of the cortex. *Neuron* 77, 388–405.
- Lewis, D.A., Curley, A.A., Glausier, J.R., and Volk, D.W. (2012). Cortical parvalbumin interneurons and cognitive dysfunction in schizophrenia. *Trends Neurosci.* 35, 57–67.
- Liodis, P., Denaxa, M., Grigoriou, M., Akufu-Addo, C., Yanagawa, Y., and Pachnis, V. (2007). Lhx6 activity is required for the normal migration and specification of cortical interneuron subtypes. *J. Neurosci.* 27, 3078–3089.
- Lodato, S., Tomassy, G.S., De Leonibus, E., Uzategui, Y.G., Andolfi, G., Armentano, M., Touzot, A., Gaztelu, J.M., Arlotta, P., Menendez de la Prida, L., and Studer, M. (2011). Loss of COUP-TFI alters the balance between caudal ganglionic eminence- and medial ganglionic eminence-derived cortical interneurons and results in resistance to epilepsy. *J. Neurosci.* 31, 4650–4662.
- Ma, T., Zhang, Q., Cai, Y., You, Y., Rubenstein, J.L., and Yang, Z. (2012). A subpopulation of dorsal lateral/caudal ganglionic eminence-derived neocortical interneurons expresses the transcription factor Sp8. *Cereb. Cortex* 22, 2120–2130.
- Macintyre, G., Alford, T., Xiong, L., Rouleau, G.A., Tibbo, P.G., and Cox, D.W. (2010). Association of NPAS3 exonic variation with schizophrenia. *Schizophr. Res.* 120, 143–149.
- Marín, O. (2012). Interneuron dysfunction in psychiatric disorders. *Nat. Rev. Neurosci.* 13, 107–120.
- Marín, O. (2013). Cellular and molecular mechanisms controlling the migration of neocortical interneurons. *Eur. J. Neurosci.* 38, 2019–2029.
- Marsh, E., Fulp, C., Gomez, E., Nasrallah, I., Minarcik, J., Sudi, J., Christian, S.L., Mancini, G., Labosky, P., Dobyns, W., et al. (2009). Targeted loss of Arx results in a developmental epilepsy mouse model and recapitulates the human phenotype in heterozygous females. *Brain* 132, 1563–1576.
- Miyoshi, G., Hjerling-Leffler, J., Karayannis, T., Sousa, V.H., Butt, S.J., Battiste, J., Johnson, J.E., Machold, R.P., and Fishell, G. (2010). Genetic fate mapping reveals that the caudal ganglionic eminence produces a large and diverse population of superficial cortical interneurons. *J. Neurosci.* 30, 1582–1594.
- Murdoch, J.D., and State, M.W. (2013). Recent developments in the genetics of autism spectrum disorders. *Curr. Opin. Genet. Dev.* 23, 310–315.
- Nóbrega-Pereira, S., Gelman, D., Bartolini, G., Pla, R., Pierani, A., and Marín, O. (2010). Origin and molecular specification of globus pallidus neurons. *J. Neurosci.* 30, 2824–2834.
- Ohshiro, T., and Saigo, K. (1997). Transcriptional regulation of breathless FGF receptor gene by binding of TRACHEALLESS/dARNT heterodimers to three central midline elements in Drosophila developing trachea. *Development* 124, 3975–3986.
- Pieper, A.A., Wu, X., Han, T.W., Estill, S.J., Dang, Q., Wu, L.C., Reece-Fincannon, S., Dudley, C.A., Richardson, J.A., Brat, D.J., and McKnight, S.L. (2005). The neuronal PAS domain protein 3 transcription factor controls FGF-mediated adult hippocampal neurogenesis in mice. *Proc. Natl. Acad. Sci. USA* 102, 14052–14057.
- Poduri, A., Evrony, G.D., Cai, X., Elhosary, P.C., Beroukhi, R., Lehtinen, M.K., Hills, L.B., Heinzen, E.L., Hill, A., Hill, R.S., et al. (2012). Somatic activation of AKT3 causes hemispheric developmental brain malformations. *Neuron* 74, 41–48.
- Rivière, J.B., Mirzaa, G.M., O’Roak, B.J., Beddaoui, M., Alcantara, D., Conway, R.L., St-Onge, J., Schwartzentruber, J.A., Gripp, K.W., Nikkel, S.M., et al. (2012). Finding of Rare Disease Genes (FORGE) Canada Consortium (2012). De novo germline and postzygotic mutations in AKT3, PIK3R2 and PIK3CA cause a spectrum of related megalencephaly syndromes. *Nat. Genet.* 44, 934–940.
- Rubenstein, J.L., and Merzenich, M.M. (2003). Model of autism: increased ratio of excitation/inhibition in key neural systems. *Genes Brain Behav.* 2, 255–267.
- Rudy, B., Fishell, G., Lee, S., and Hjerling-Leffler, J. (2011). Three groups of interneurons account for nearly 100% of neocortical GABAergic neurons. *Dev. Neurobiol.* 71, 45–61.
- Silbereis, J.C., Nobuta, H., Tsai, H.H., Heine, V.M., McKinsey, G.L., Meijer, D.H., Howard, M.A., Petryniak, M.A., Potter, G.B., Alberta, J.A., et al. (2014). Olig1 function is required to repress dlx1/2 and interneuron production in Mammalian brain. *Neuron* 81, 574–587.
- Southwell, D.G., Paredes, M.F., Galvao, R.P., Jones, D.L., Froemke, R.C., Sebe, J.Y., Alfaro-Cervello, C., Tang, Y., Garcia-Verdugo, J.M., Rubenstein, J.L., et al. (2012). Intrinsically determined cell death of developing cortical interneurons. *Nature* 491, 109–113.
- Striano, P., and Zara, F. (2012). Genetics: mutations in mTOR pathway linked to megalencephaly syndromes. *Nat. Rev. Neurol.* 8, 542–544.
- Sussel, L., Marín, O., Kimura, S., and Rubenstein, J.L. (1999). Loss of Nkx2.1 homeobox gene function results in a ventral to dorsal molecular respecification within the basal telencephalon: evidence for a transformation of the pallidum into the striatum. *Development* 126, 3359–3370.
- Tamamaki, N., Yanagawa, Y., Tomioka, R., Miyazaki, J., Obata, K., and Kaneko, T. (2003). Green fluorescent protein expression and colocalization with calretinin, parvalbumin, and somatostatin in the GAD67-GFP knock-in mouse. *J. Comp. Neurol.* 467, 60–79.
- Taniguchi, H., Lu, J., and Huang, Z.J. (2013). The spatial and temporal origin of chandelier cells in mouse neocortex. *Science* 339, 70–74.
- Visel, A., Taher, L., Girgis, H., May, D., Golonzhka, O., Hoch, R.V., McKinsey, G.L., Pattabiraman, K., Silberberg, S.N., Blow, M.J., et al. (2013). A high-resolution enhancer atlas of the developing telencephalon. *Cell* 152, 895–908.
- Yizhar, O., Fenno, L.E., Prigge, M., Schneider, F., Davidson, T.J., O’Shea, D.J., Sohal, V.S., Goshen, I., Finkelstein, J., Paz, J.T., et al. (2011). Neocortical

excitation/inhibition balance in information processing and social dysfunction. *Nature* 477, 171–178.

Zhao, Y., Flandin, P., Long, J.E., Cuesta, M.D., Westphal, H., and Rubenstein, J.L.R. (2008). Distinct molecular pathways for development of telencephalic interneuron subtypes revealed through analysis of *Lhx6* mutants. *J. Comp. Neurol.* 510, 79–99.

Zhou, J., and Parada, L.F. (2012). PTEN signaling in autism spectrum disorders. *Curr. Opin. Neurobiol.* 22, 873–879.

Zhou, Y.D., Barnard, M., Tian, H., Li, X., Ring, H.Z., Francke, U., Shelton, J., Richardson, J., Russell, D.W., and McKnight, S.L. (1997). Molecular characterization of two mammalian bHLH-PAS domain proteins selectively expressed in the central nervous system. *Proc. Natl. Acad. Sci. USA* 94, 713–718.

Neuron, Volume 84

## **Supplemental Information**

### **NPAS1 Represses the Generation of Specific Subtypes of Cortical Interneurons**

Amelia Stanco, Ramón Pla, Daniel Vogt, Yiran Chen, Shyamali Mandal, Jamie Walker, Robert F. Hunt, Susan Lindtner, Carolyn A. Erdman, Andrew A. Pieper, Steven P. Hamilton, Duan Xu, Scott C. Baraban, and John L.R. Rubenstein

## Supplemental Data

**Figure S1, related to Figure 1. Co-localization analysis of interneuron marker and NPAS1 or NPAS3 expression at P0, P5, and P15.** NPAS1 or NPAS3 protein co-immunofluorescence with GFP (from *GAD67-GFP* or *Lhx6-GFP* alleles) or interneuron markers (i.e., reelin, SST, CR, or PV) in coronal sections of the somatosensory cortex at P0, P5, and P15. **(A and B)** At P0, virtually all NPAS1<sup>+</sup> cells express *GAD67-GFP* (A), whereas 30% co-express *Lhx6-GFP* (B). Arrowheads show NPAS1<sup>+</sup>/Lhx6-GFP<sup>-</sup> cells. **(C and D)** Nearly all developing cortical NPAS1<sup>+</sup> cells (C) or the majority of NPAS3<sup>+</sup> cells (D) express *GAD67-GFP* at P5. **(E to L)** At P15, NPAS1 and NPAS3 are expressed by a majority of reelin<sup>+</sup> (E and I) and SST<sup>+</sup> (F and J) interneurons. NPAS3 is expressed by a small fraction of PV<sup>+</sup> cells (L), while NPAS1 expression is nearly absent from PV<sup>+</sup> cells (H). *n* = 3 animals for (A) to (L). Scale bar, (A) and (B) 150  $\mu$ m; (C) and (D) 350  $\mu$ m; (E) to (L) 230  $\mu$ m.

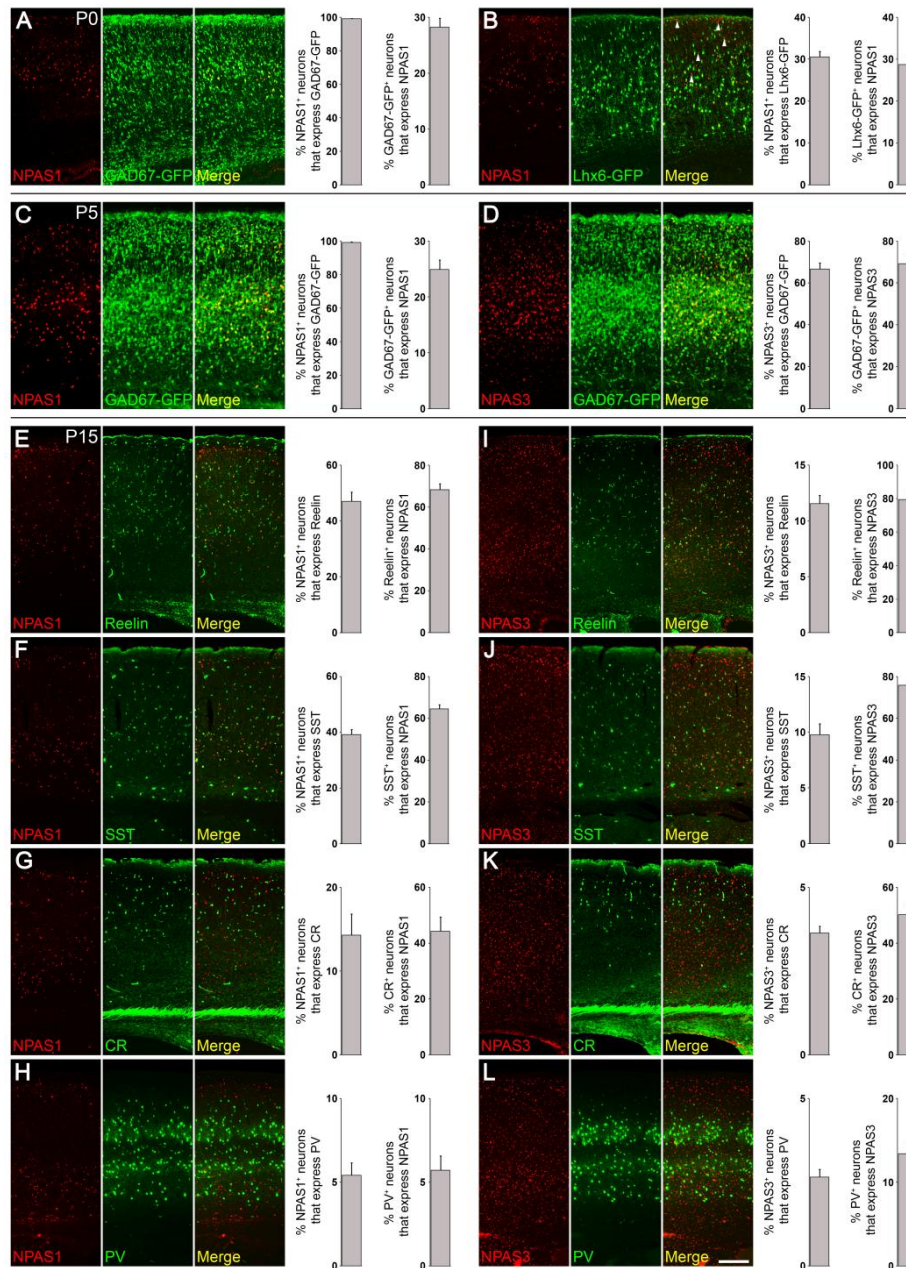


**Figure S2, related to Figure 1. Co-localization analysis of interneuron marker and NPAS1 or NPAS3 expression at P30.** NPAS1 or NPAS3 protein co-immunofluorescence with GFP (from the *GAD67-GFP* allele) or interneuron markers (i.e., reelin, SST, CR, or PV) in coronal sections of the somatosensory cortex at P30. (A to J) By P30, most NPAS1<sup>+</sup> cells express *GAD67-GFP* (A), whereas 21% of NPAS3<sup>+</sup> cells express *GAD67-GFP* (F). NPAS1 is expressed predominantly in reelin<sup>+</sup> (B), SST<sup>+</sup> (C), and CR<sup>+</sup> (D) interneurons and rare in PV<sup>+</sup> (E) cells. A large proportion of all interneuron subtypes examined express NPAS3 at P30 (G to J). *n* = 3 animals for (A) to (J). Scale bar, (A) to (J) 220  $\mu$ m.

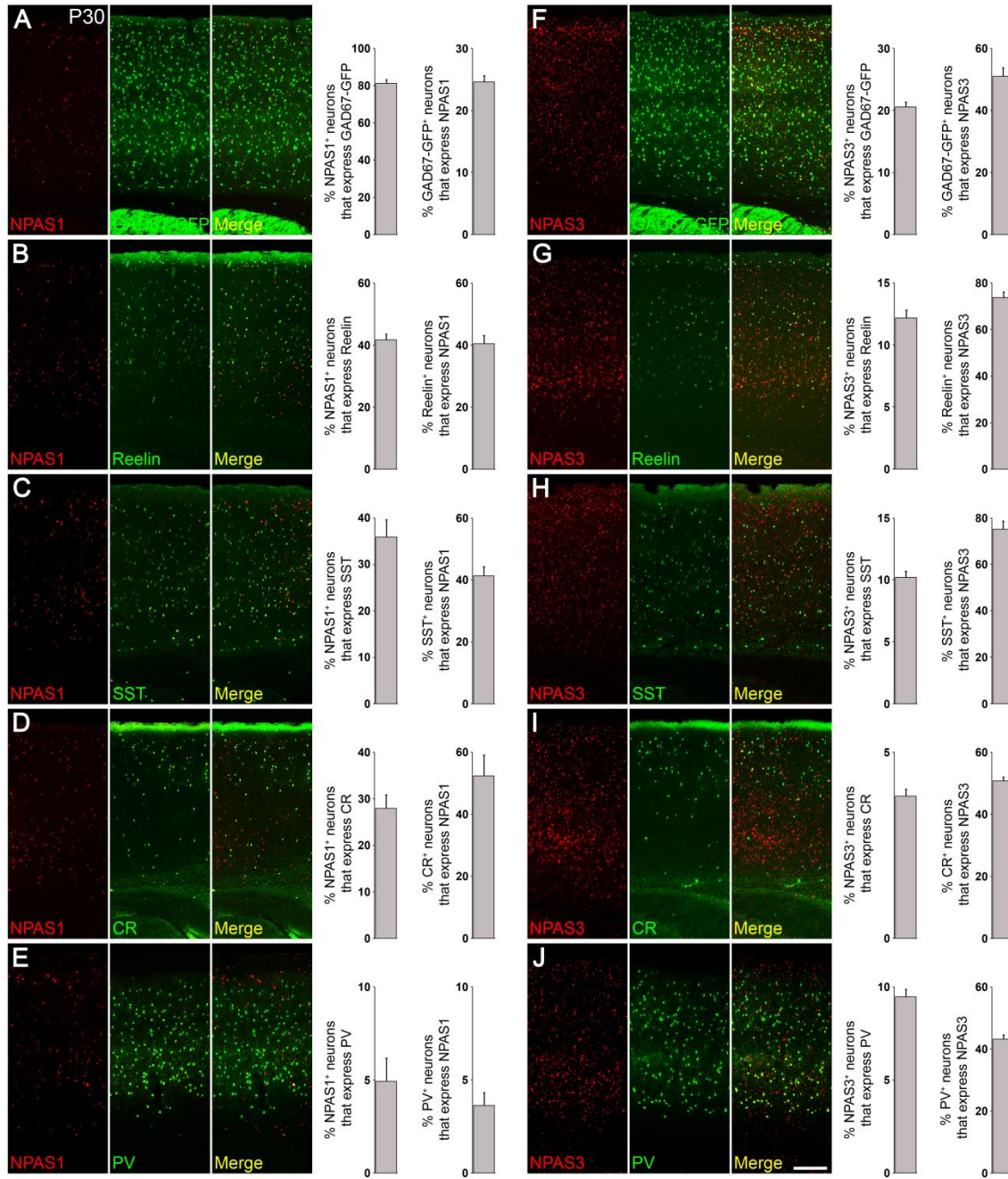


**Figure S3, related to Figure 2. Interneuron apoptosis and cortical volume is increased in the *NPAS1*<sup>-/-</sup> somatosensory cortex, while the *NPAS3*<sup>-/-</sup> cortex exhibits a decrease in cortical volume and no change in apoptosis.** (A) Increased interneuron (*GAD67-GFP*) apoptosis (activated caspase-3<sup>+</sup> cells) at P7 in the *NPAS1*<sup>-/-</sup> somatosensory cortex based on a co-immunofluorescence assay. Arrowheads show *GAD67-GFP*<sup>+</sup>/activated caspase-3<sup>+</sup> cells. (B and C) Quantification of *GAD67-GFP*<sup>+</sup>/activated caspase-3<sup>+</sup> or activated caspase-3<sup>+</sup> cells at P7 in *NPAS1*<sup>-/-</sup> (B) or *NPAS3*<sup>-/-</sup> (C) mutants, respectively. *n* = 3 animals per genotype for (B) and (C). (D and F) Increased cortical (rostral and middle) volume in P30 *NPAS1*<sup>-/-</sup> mutants based on measurements of Nissl-stained coronal sections (D) and MRI data (F). Boxed areas in (D) are shown in higher magnification. (F) Illustration of cortical and basal ganglia regions used for volume calculations. (E, G and H) Cortical width (E) and cortical and basal ganglia volume (G and H) measurements. *n* = 3 animals per genotype for (E), (G), and (H). \**P* < 0.05. \*\**P* < 0.01. \*\*\**P* < 0.001. Scale bars, (A) 300 μm; (D) 2 mm (low magnification images), 740 μm (high magnification images); (F) 2 mm.

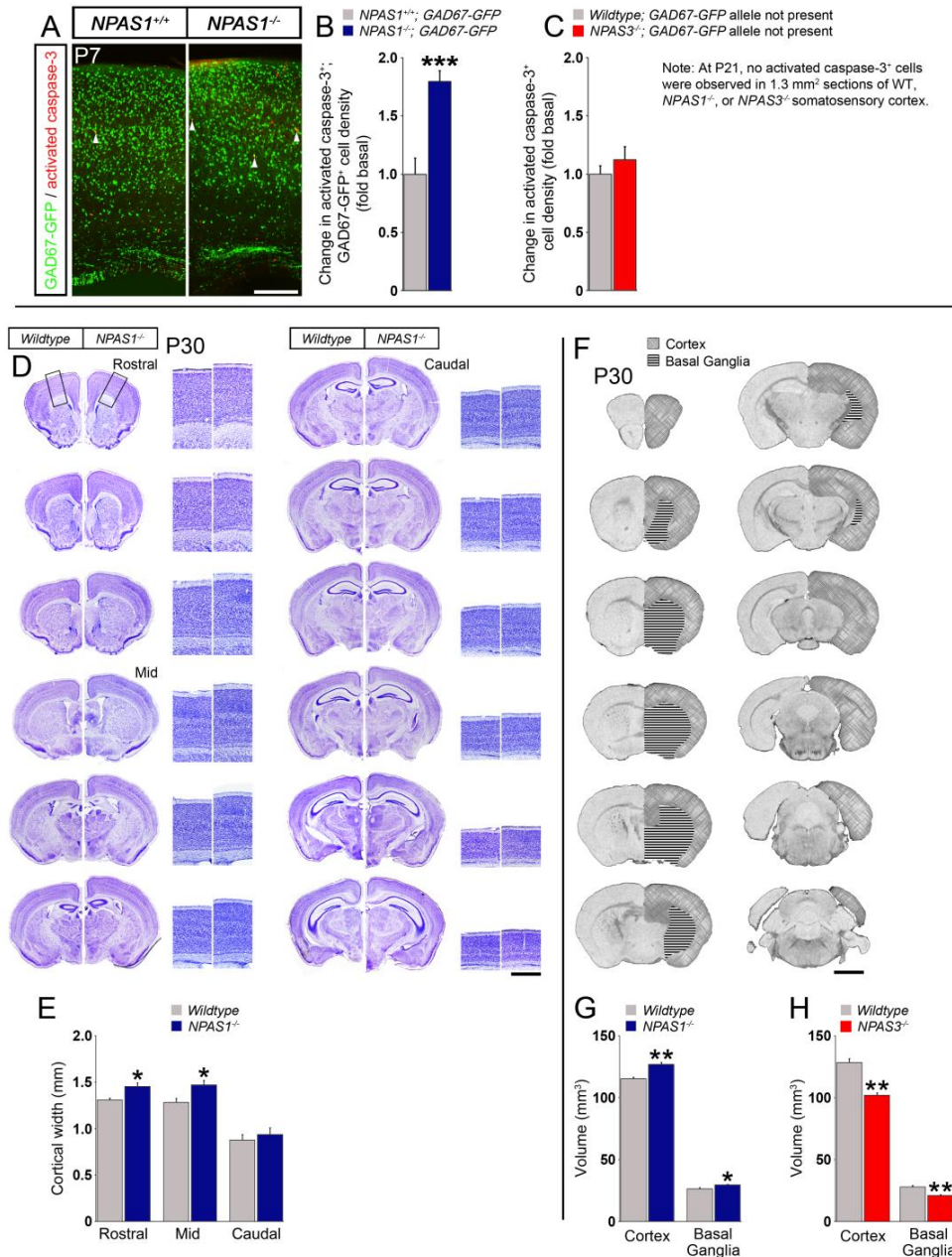


**Figure S4, related to Figure 4. The neocortex of *NPAS1*<sup>-/-</sup> has layer-specific increases in numbers and density of NeuN<sup>+</sup> and GAD67-GFP<sup>+</sup> neurons. (A) Increase in NeuN<sup>+</sup> neurons (somatosensory Cx) at P21 shown on coronal cortical sections in *NPAS1*<sup>-/-</sup> mice. (B to D) Quantification of NeuN<sup>+</sup> neurons/10<sup>4</sup> μm<sup>2</sup> (B), GAD67-GFP<sup>+</sup> neurons/10<sup>4</sup> μm<sup>2</sup> (C), and NeuN<sup>+</sup> and GAD67-GFP<sup>+</sup>/GAD67-GFP<sup>+</sup> ratio (D) in somatosensory cortex and individual layers (yellow lines) at P21. *n* = 3 animals per genotype for (B) to (D). (E) Representative immunohistochemical staining of the cerebral cortex for NeuN and GAD67 in 3 month old mice reveals an increase in the density of all neurons as well as inhibitory interneurons in *NPAS1*<sup>-/-</sup> mutants. (F and G) Stereological quantification of NeuN<sup>+</sup> neurons/1 mm<sup>3</sup> cerebral cortex (F) and GAD67<sup>+</sup> neurons/1 mm<sup>3</sup> cerebral cortex (G) in *NPAS1*-deficient mice at 3 months of age. *n* = 5 wildtype and 7 *NPAS1*<sup>-/-</sup> mutant animals for (F) and (G). (H) Density of layer-specific cortical pyramidal cells is unaltered in *NPAS1*<sup>-/-</sup> mutants based on Cux1<sup>+</sup> (layer II/III), Ctip2<sup>+</sup> (layer V), and Tbr1<sup>+</sup> (layer VI) immunofluorescence staining of coronal sections from P21 somatosensory cortex. There are no significant changes in the density of Cux1<sup>+</sup> or Ctip2<sup>+</sup> cells in *NPAS3*<sup>-/-</sup> mutant mice. However, *NPAS3*<sup>-/-</sup> mutants displayed a 16% (16 ± 3.05%, *p* = 0.0001) increase in Tbr1<sup>+</sup> cell density. (I to K) Quantification of Cux1<sup>+</sup> (I), Ctip2<sup>+</sup> (J), and Tbr1<sup>+</sup> (K) neurons/10<sup>4</sup> μm<sup>2</sup> of somatosensory cortex. *n* = 3 animals per genotype for (I) to (K). Abbreviations: Cx: cortex. \**P* < 0.05. \*\**P* < 0.01. \*\*\**P* < 0.001. Scale bars, (A) 300 μm; (E) 100 μm; (H) 300 μm.**

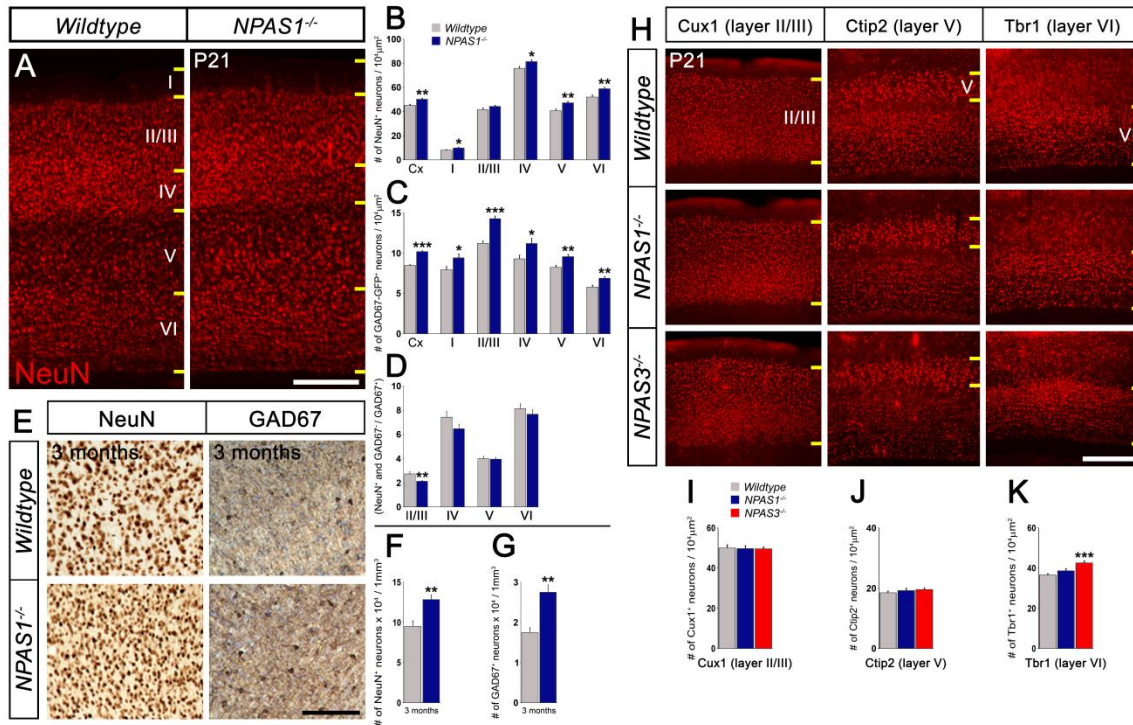


**Figure S5, related to Figure 5. *NPAS1*<sup>-/-</sup> mutant mice show increased neurogenesis in the ganglionic eminence and hippocampus, while *NPAS3*<sup>-/-</sup> mutants exhibit decreased neurogenesis in the ganglionic eminence. (A) BrdU immunofluorescence staining of E13.5 coronal sections following 1 hr BrdU pulse labeling reveals increased neurogenesis in the subventricular zone of the *NPAS1*<sup>-/-</sup> mutant MGE and CGE, whereas *NPAS3*<sup>-/-</sup> mutant mice display reduced neurogenesis in the MGE subventricular zone. (B to E) Quantification of BrdU<sup>+</sup> cell density (C and E) and total cell number (B and D) in ventricular and subventricular zones of the E13.5 MGE (B and C) and CGE (D and E). *n* = 3 animals per genotype for (B) to (E). (F) Increased BrdU<sup>+</sup> cells in the hippocampal dentate gyrus of 5-10 week old *NPAS1*<sup>-/-</sup> mice following intraperitoneal injection of BrdU once daily for 12 days. (G) Quantification of BrdU<sup>+</sup> cells/1 mm<sup>3</sup> hippocampal dentate gyrus. For (G), *n* = 22 wildtype and 28 *NPAS1*<sup>-/-</sup> mutant animals. Abbreviations: CGE: caudal ganglionic eminence, MGE: medial ganglionic eminence, SVZ: subventricular zone, VZ: ventricular zone. \**P* < 0.05. \*\**P* < 0.01. \*\*\**P* < 0.001. Scale bars, (A) 150 μm; (F) 250 μm.**

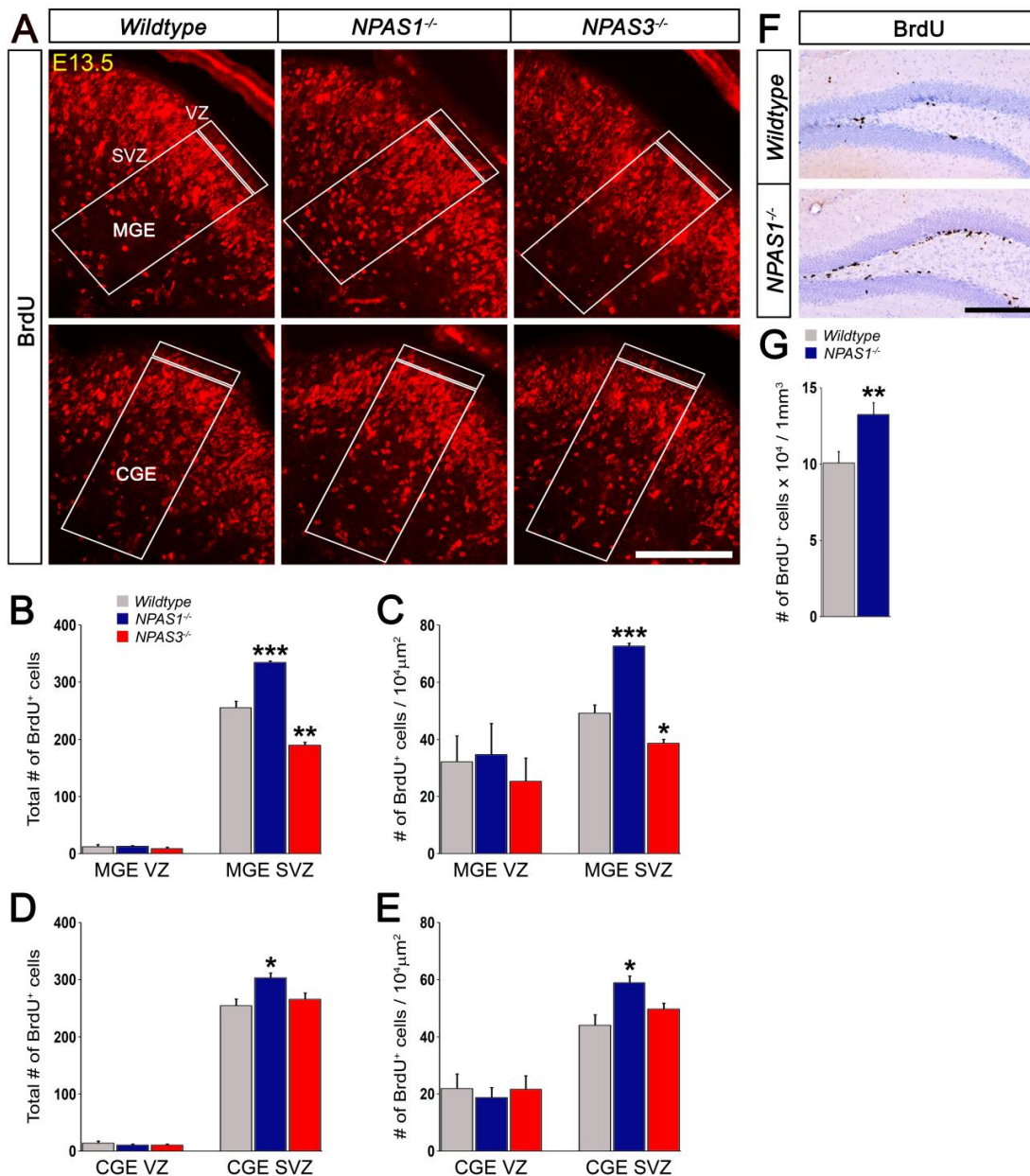


**Figure S6, related to Figure 6. ISH assay of regulatory genes in *NPAS1*<sup>-/-</sup> mutants.** (A to L) RNA expression of most genes that we studied did not change at E13.5 (A to F) and E15.5 (G to L) in the MGE and CGE of *NPAS1*<sup>-/-</sup> mutants. Data presented in coronal sections at three rostro-caudal planes (left to right). Scale bar, (A) to (F) 800  $\mu$ m; (G) to (L) 1 mm.

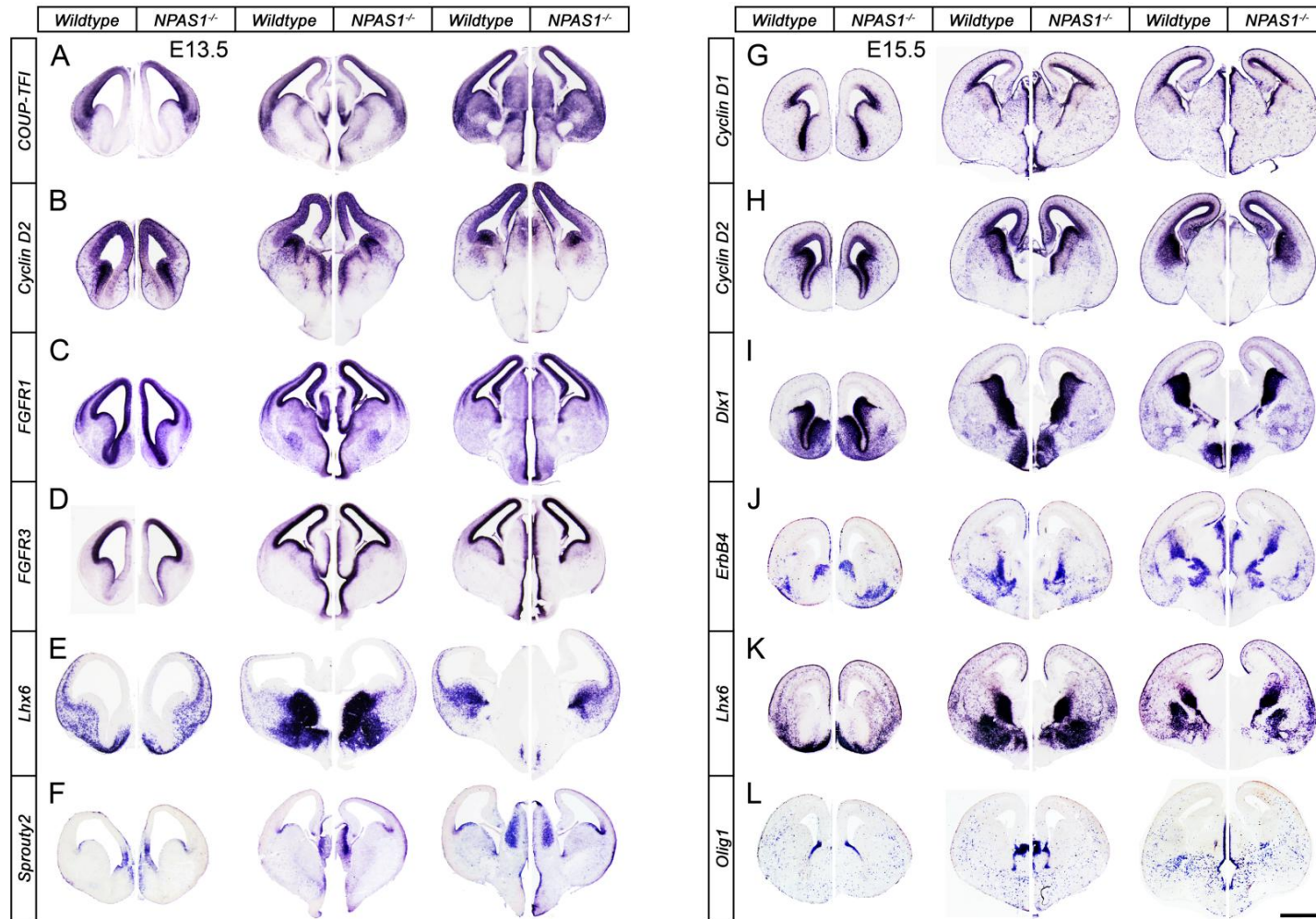


**Figure S7, related to Figure 7. Increased Arx expression in the CGE mediates increased subpallial MAP kinase activity.** (A) Arx over-expression in the dorsal LGE/CGE VZ (arrowheads) two days after *in utero* injection of a *CMV-GFP-T2a-Arx* lentivirus. Compare the left (non-injected) and right (*CMV-GFP-T2a-Arx*-injected) hemisphere. This is a section of the dorsal LGE/CGE taken from the same brain series used to illustrate Arx (from *CMV-GFP-T2a-Arx*) and PH3 co-expression in Figure 7A. (B and C) *In utero* lentiviral transduction of Arx into the E13.5 CGE results in increased MAP kinase activity (phospho-ERK). Phospho-ERK levels in the CGE/MGE (white box) were normalized by comparison with cortical levels (yellow box). Asterisks in (B) indicate that phospho-ERK immunohistochemistry panels contain a blood vessel staining artifact.  $n = 3$  animals per experimental condition for (C). (D) Arx locus showing evolutionarily conserved domains, one of which is a subpallial enhancer (*UAS3*) (Colasante et al., 2008; Visel et al., 2013) that has two predicted *NPAS1/ARNT* sites (Hogenesch et al., 1997). Abbreviations: CGE: caudal ganglionic eminence, Cx: cortex. \* $P < 0.05$ . Scale bars, (A) 500  $\mu\text{m}$ ; (B) 120  $\mu\text{m}$ .

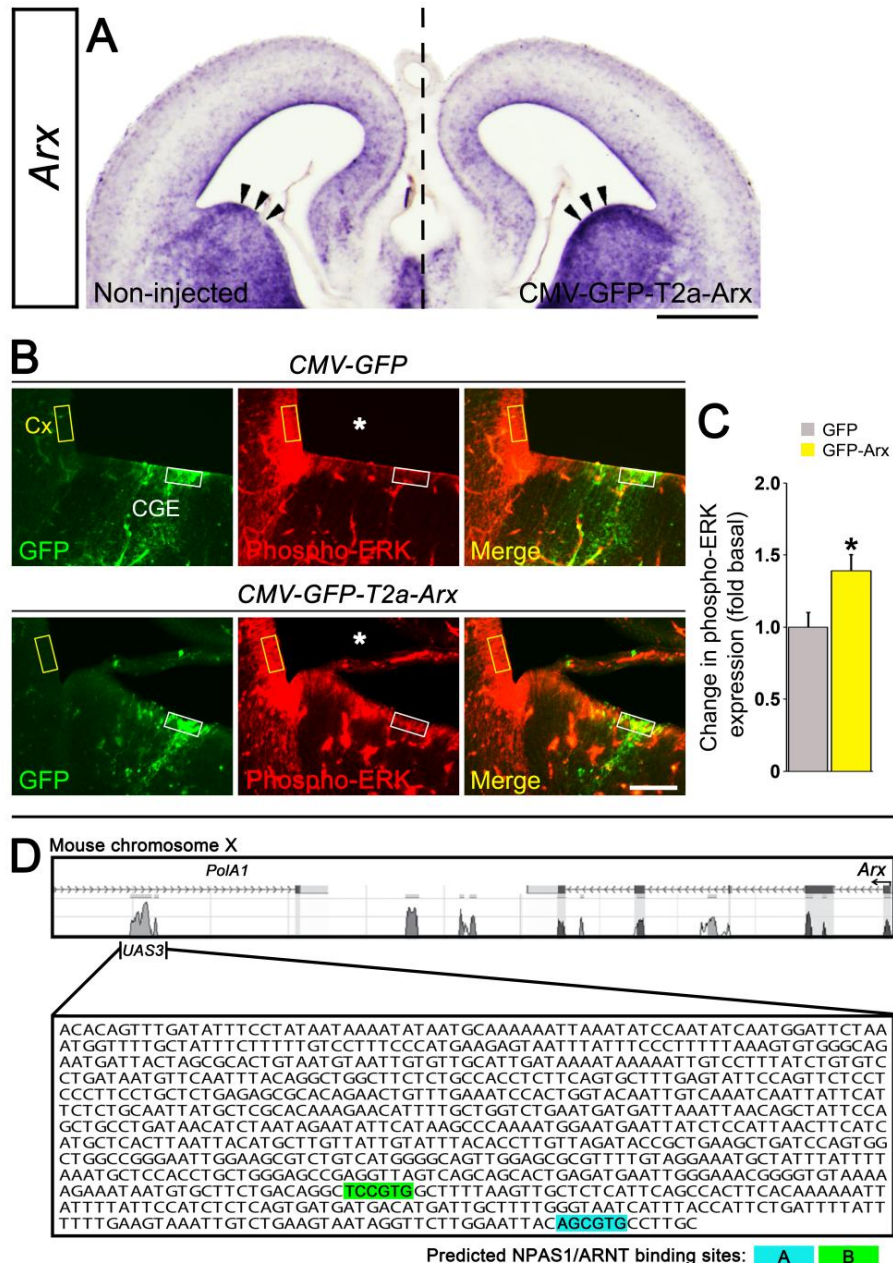


**Table S1. Percentage of NPAS1<sup>+</sup> or NPAS3<sup>+</sup> neurons that express various interneuron markers.**

<b>Interneuron Marker</b>	<b>Age</b>	<b>NPAS1</b>	<b>NPAS3</b>
GAD67-GFP	P0	99%	N/A
GAD67-GFP	P5	99%	67%
GAD67-GFP	P30	81%	21%
Lhx6-GFP	P0	31%	N/A
Reelin	P15	47%	12%
Reelin	P30	42%	12%
Somatostatin	P15	39%	10%
Somatostatin	P30	36%	10%
Calretinin	P15	14%	4%
Calretinin	P30	28%	4%
Parvalbumin	P15	5%	3%
Parvalbumin	P30	5%	9%

**Table S2. Percentage of interneuron marker<sup>+</sup> neurons that express NPAS1 or NPAS3.**

<b>Interneuron Marker</b>	<b>Age</b>	<b>NPAS1</b>	<b>NPAS3</b>
GAD67-GFP	P0	28%	N/A
GAD67-GFP	P5	25%	69%
GAD67-GFP	P30	25%	51%
Lhx6-GFP	P0	29%	N/A
Reelin	P15	68%	79%
Reelin	P30	40%	74%
Somatostatin	P15	65%	76%
Somatostatin	P30	41%	75%
Calretinin	P15	44%	50%
Calretinin	P30	52%	51%
Parvalbumin	P15	6%	13%
Parvalbumin	P30	4%	43%

**Table S3. MRI quantification of P30 cortical and basal ganglia volumes in control, *NPAS1*<sup>-/-</sup>, and *NPAS3*<sup>-/-</sup>.**

<b>Genotype</b>	<b>Cortex (mm<sup>3</sup>)</b>	<b>Basal Ganglia (mm<sup>3</sup>)</b>
<i>Wildtype</i>	115.510	27.158
<i>Wildtype</i>	117.296	24.663
<i>Wildtype</i>	112.638	27.250
<i>NPAS1</i> <sup>-/-</sup>	127.270	28.916
<i>NPAS1</i> <sup>-/-</sup>	129.407	29.387
<i>NPAS1</i> <sup>-/-</sup>	123.904	30.463
<i>Wildtype</i>	134.158	30.003
<i>Wildtype</i>	126.982	27.299
<i>Wildtype</i>	123.636	26.548
<i>NPAS3</i> <sup>-/-</sup>	100.941	22.214
<i>NPAS3</i> <sup>-/-</sup>	105.621	20.867
<i>NPAS3</i> <sup>-/-</sup>	99.332	20.066

## **Supplemental Experimental Procedures**

### **Tissue preparation**

Mice were deeply anesthetized and perfused intracardially with 4% paraformaldehyde (PFA) in 1X phosphate-buffered saline solution (PBS, pH 7.4). The brains were removed and post-fixed overnight in the same fixative. As an exception, brains prepared for VIP immunohistochemistry were post-fixed for 30 min and stored in 1X PBS. The following day, tissue was vibratome sectioned (50  $\mu$ m) and used either for *in situ* hybridization, immunohistochemistry, or Nissl stain analysis.

### ***In Situ* hybridization**

Section *in situ* hybridization experiments were performed using digoxigenin riboprobes on 50  $\mu$ m sections as described previously (Jeong et al., 2008).

### **Immunohistochemistry**

Brain sections were prepared at a thickness of 50  $\mu$ m on a vibratome and used for immunohistochemistry. The slices were washed in 1X PBS, incubated in blocking solution (5% bovine serum albumin, 3% normal goat serum, 0.3% Triton X-100 in PBS or 5% bovine serum albumin, 0.3% Triton X-100 in PBS for ChAT IHC) for 1 hour, and incubated overnight at 4°C in the primary antibody diluted in blocking solution. Antigen unmasking procedures were performed on mounted tissue sections for BrdU, ChAT, and Ctip2 immunohistochemistry prior to the blocking step. For ChAT and Ctip2 IHC, sections were boiled for 20 min in 10 mM sodium citrate and 0.05% Tween 20, pH 6, cooled at RT for 20 min, and rinsed briefly in 1X PBS. For BrdU labeling of embryonic tissue, sections were incubated in 4 N HCl for 45 min at 42°C, followed by a 10 min incubation in 0.1 M sodium borate, pH 8.5, and rinsed three times for 10 min in 1X PBS. For BrdU labeling of postnatal tissue, sections were incubated for 2 h in 50%

formamide/2X saline sodium citrate (SSC) at 65°C, followed by a 5 min wash in 2X SSC and subsequent incubation for 30 min in 2 M HCl at 37°C. The antibodies used were as follows: rabbit anti-NPAS1 (1:500; gift from Steven McKnight), rabbit anti-NPAS3 (1:500; gift from Steven McKnight), chicken anti-GFP (1:2000, Aves Labs), rabbit anti-VIP (1:200, ImmunoStar), mouse anti-reelin (1:500, Millipore), rabbit anti-NPY (1:250, ImmunoStar), sheep anti-NPY (1:1000, Millipore), mouse anti-parvalbumin (1:500, Millipore), mouse anti-calretinin (1:500, Swant), rat anti-SST (1:200, Millipore), goat anti-ChAT (1:100, Millipore), rabbit anti-PH3 (1:500, Millipore), rabbit anti-phospho-ERK (1:100, Cell Signaling Technology), rabbit anti-cleaved caspase-3 (1:500, Cell Signaling Technology), mouse anti-NeuN (1:500, Millipore), mouse anti-GAD67 (1:1000, Millipore), rabbit anti-Cux1 (1:100, Santa Cruz Biotechnology), rat anti-Ctip2 (1:500, Abcam), rabbit anti-Tbr1 (1:500, Abcam), rat anti-BrdU (1:100, Abcam), mouse anti-BrdU (1:100, Roche), rabbit anti-Ki-67 (1:250, Abcam). Immunoreactivity was detected with appropriate Alexa-488 or Alexa-594 (1:300, Molecular Probes) conjugated secondary antibodies or biotinylated secondary antibodies used in conjunction with ABC reagent and diaminobenzidine (Vector Laboratories) for chromogenic detection of the marker.

### **BrdU labeling**

Proliferation of E13.5 ventricular and subventricular zone cells within the medial and caudal ganglionic eminences was assessed by single intraperitoneal injections of BrdU (50 mg/kg; Sigma–Aldrich) performed following standard procedures. Basal levels of neural precursor cell proliferation in dentate gyrus subgranular zone (SGZ) were determined in mice 5-10 weeks of age. These mice were housed individually in standard cages with *ad libitum* access to food and water and were intraperitoneal injected once daily with BrdU (50 mg/kg) for 12 days. Animals were deeply anesthetized 1 hour after BrdU injection for GE cell proliferation analysis or on day 13 for dentate gyrus SGZ cell

proliferation analysis, immediately perfused, and brain tissue processed for immunohistochemical staining with BrdU antibodies.

### **Quantification**

With the exception of co-expression and hippocampal BrdU analysis, quantification was performed on images obtained with a CoolSNAP EZ Turbo 1394 digital camera (Photometric) on a Nikon ECLIPSE 80i microscope (Nikon Instruments Inc.) using a 10X or 4X objective. Image analysis of BrdU-labeled ganglionic eminences, NeuN<sup>+</sup>/GAD67-GFP<sup>+</sup> and cleaved caspase-3<sup>+</sup>/GAD67-GFP<sup>+</sup> co-expression as well as NPAS1 or NPAS3 co-expression with GAD67-GFP, Lhx6-GFP, reelin, SST, CR, PV, or NPY was carried out on images obtained with a confocal microscope (LSM 510 META NLO, Carl Zeiss International) with a 10X or 20X objective. Results were determined in five coronal sections from three mice of each genotype. Quantification of BrdU-labeled proliferating neural precursor cells in the hippocampal dentate gyrus subgranular zone was performed on images acquired with a Nikon ECLIPSE 90i motorized microscope coupled with MetaMorph Image Acquisition software (Molecular Devices). BrdU<sup>+</sup> cells within the dentate gyrus SGZ were counted in every third section of both hemispheres (~10–15 sections per animal) for 22 wildtype and 28 *NPAS1*<sup>-/-</sup> mutant mice.

Quantification of GAD67-GFP<sup>+</sup>, VIP<sup>+</sup>, reelin<sup>+</sup>, NPY<sup>+</sup>, PV<sup>+</sup>, SST<sup>+</sup>, and NeuN<sup>+</sup> cells was carried out in primary somatosensory cortex. The numbers of positive cells were assessed in a 225,000  $\mu\text{m}^2$ , 350,000  $\mu\text{m}^2$ , 400,000  $\mu\text{m}^2$ , or 1 mm<sup>2</sup> area of E15.5, E17.5, P0, or P30 somatosensory cortex, respectively. The numbers of GAD67-GFP<sup>+</sup> cells within the intermediate zone of the E15.5 somatosensory cortex were determined in a 75,000  $\mu\text{m}^2$  area. The numbers of NeuN<sup>+</sup> and GAD67-GFP<sup>+</sup> cells were quantified in a 370,000  $\mu\text{m}^2$  area of P21 somatosensory cortex (layer I: 30,000  $\mu\text{m}^2$ , layer II/III: 100,000

$\mu\text{m}^2$ , layer IV: 40,000  $\mu\text{m}^2$ , layer V: 100,000  $\mu\text{m}^2$ , layer VI: 100,000  $\mu\text{m}^2$ ). Results are presented as mean  $\pm$  SEM. Statistical differences between experimental groups were determined with the Student's *t*-test or one-way ANOVA and Tukey-Kramer post hoc test using SPSS 15 software (IBM).

The numbers of PH3<sup>+</sup> cells in the E13.5 CGE and E15.5 MGE ventricular or subventricular zones were assessed in a 15,000  $\mu\text{m}^2$  or 25,000  $\mu\text{m}^2$  area, respectively. Phospho-ERK expression levels were measured with the aid of Adobe Photoshop CS4 software as a ratio of the integrated density of phospho-ERK<sup>+</sup> MGE or CGE ventricular zone cells in a 4,000  $\mu\text{m}^2$  area to the integrated density of phospho-ERK<sup>+</sup> cortical ventricular zone cells in a 4,000  $\mu\text{m}^2$  area. Integrated density is determined as the sum of the pixel values in a selected area. Results were calculated as mean  $\pm$  SEM and presented as fold change relative to control. Statistical differences between experimental groups were determined with the Student's *t*-test using SPSS 15 software (IBM).

NPAS1 or NPAS3 co-expression analysis with interneuron markers including GAD67-GFP, Lhx6-GFP, reelin, SST, CR, PV, and NPY was performed in a 400,000  $\mu\text{m}^2$ , 200,000  $\mu\text{m}^2$ , 550,000  $\mu\text{m}^2$ , or 650,000  $\mu\text{m}^2$  area of P0, P5, P15, or P30 somatosensory cortex, respectively. NeuN<sup>+</sup>/GAD67-GFP<sup>+</sup> co-expression was quantified in a 100,000  $\mu\text{m}^2$ , 40,000  $\mu\text{m}^2$ , 100,000  $\mu\text{m}^2$ , or 100,000  $\mu\text{m}^2$  area of layer II/III, IV, V, or VI P21 somatosensory cortex, respectively. Results are expressed as mean  $\pm$  SEM. Cleaved caspase-3<sup>+</sup>/GAD67-GFP<sup>+</sup> co-expression or the numbers of cleaved caspase-3<sup>+</sup> cells alone were quantified in a 1 mm<sup>2</sup> area of P7 somatosensory cortex. Results were calculated as mean  $\pm$  SEM and presented as fold change relative to control. Statistical differences between experimental groups were assessed with the Student's *t*-test using SPSS 15 software (IBM). The percentage of NPAS1<sup>+</sup> or NPAS3<sup>+</sup> neurons that express

various interneuron markers and vice versa are reported in tables in the Supplemental Experimental Procedures (see below).

The numbers of Cux1<sup>+</sup>, Ctip2<sup>+</sup>, or Tbr1<sup>+</sup> cells in the P21 somatosensory cortex were analyzed in a 100,000  $\mu\text{m}^2$ , 60,000  $\mu\text{m}^2$  or 60,000  $\mu\text{m}^2$  area, respectively. Results are presented as mean  $\pm$  SEM. Statistical differences between experimental groups were determined with the one-way ANOVA and Tukey-Kramer post hoc test using SPSS 15 software (IBM).

Quantification of BrdU<sup>+</sup> cell density and total cell number in the E13.5 MGE and CGE ventricular and subventricular zones was performed by defining these regions using Ki-67 co-immunohistochemistry. BrdU<sup>+</sup> cell density in ventricular or subventricular zones was determined in a 4,000  $\mu\text{m}^2$  or 35,000  $\mu\text{m}^2$  area, respectively. The numbers of basal *in vivo* BrdU-labeled proliferating neural precursor cells in the dentate gyrus subgranular zone were assessed in 5-10 week old mice. Immunopositive cells in the SGZ, defined as a two-cell-body-wide zone of the hilus along the base of the granular layer of the dentate gyrus, were counted in every third section of both hemispheres (~10–15 sections per animal) progressing posteriorly from the point where the supra-pyramidal and infra-pyramidal blades are joined at the crest region and the dentate gyrus is oriented horizontally beneath the corpus callosum. Quantification of immunopositive cells was performed by separate investigators in a blinded manner. Results are presented as mean  $\pm$  SEM. Statistical differences between experimental groups were assessed with the Student's *t*-test or one-way ANOVA and Tukey-Kramer post hoc test using SPSS 15 software (IBM).

## **Stereology**

Stereological quantification of NeuN<sup>+</sup> and GAD67<sup>+</sup> cells within the cerebral cortex was performed using Stereologer 2000 software (SRC). The numbers of NeuN<sup>+</sup> and GAD67<sup>+</sup> cells were analyzed at 3 months of age.  $n = 5$  wildtype and 7 *NPAS1*<sup>-/-</sup> mutant animals. For each animal, 10 sections were analyzed. Cells were counted in a specified area in several random positions throughout each section. Results are expressed as mean  $\pm$  SEM. Statistical differences between experimental groups were determined with the Student's *t*-test using SPSS 15 software (IBM).

### **Nissl staining**

Mounted P30 coronal sections were placed in 1:1 chloroform/100% ethanol for 1 hr, rehydrated through an ethanol series, and incubated in 0.05% thionin solution for 2-2.5 min. These sections were then differentiated through an ethanol series, cleared in xylenes, and coverslipped with Permount. Neocortical width was measured from the pial surface to the dorsal limit of the white matter in a rostro-caudal series of 12 coronal sections from three mice of each genotype. Results are presented as mean  $\pm$  SEM. Statistical differences between experimental groups were determined with the Student's *t*-test using SPSS 15 software (IBM).

### **DNA vectors**

#### *Lentiviral vectors*

Mouse full length cDNA for Arx (Origene) was PCR amplified with primers (5' GAGAGCA TGCATGAGCAATCAGTACCAGG, 3' GAGAGCATGCTTAGCACACCTCCTTCCC) with introduced SphI sites, and ligated 3' to the T2a sequence in a CMV-GFP-T2a-mcs vector (gift from Miguel Ramalho-Santos) to generate CMV-GFP-T2a-Arx.

### *Expression and luciferase reporter vectors*

CMV-ARNT and CMV-NPAS1 were gifts from Steven McKnight and the CMV-GFP vector has been previously described (Flandin et al., 2011). The mouse UAS3 enhancer (Colasante et al., 2008) was PCR amplified (primers: 5' GAGAGGTACCGCAAGGCACG CTGTAATTC, 3' GAGAAGATCTACACAGTTTGATATTTC) with introduced KpnI and BglII restriction sites and ligated into the multiple cloning site of the PGL4.23-luciferase vector (Promega). The putative ARNT binding sites in the UAS3 enhancer were mutated by PCR site-directed mutagenesis using the UAS3-PGL4.23-luciferase vector as a template and the following primers: (Site A: 5' GAAAAAAGCAAGG**AAAAA**AGTAATTCC AAGAAC, 3' GTTCTTGGAATTACT**TTTTT**CCTTGCTTTTTTC) and (Site B: 5' GAGCAACTTAAAAGC**AAAAA**AGCCTGTCAGAAGC, 3' GCTTCTGACAGGC**TTTTT** GCTTTTAAGTTGCTC). Nucleotides in bold are introduced nucleotide mutations. After confirming the mutagenesis via sequencing, the mutant UAS3 enhancers were restriction digested with KpnI and BglII and subcloned into a new PGL4.23-luciferase vector at these sites.

### **Human DNA sequencing**

#### *Patients*

Autism sample details: We used autism primarily Caucasian probands from two primary sources: a) autism samples of the Simons Simplex Collection (SSC) from the Simons Foundation Autism Research Initiative (Fischbach and Lord, 2010). The phenotype is derived from the Autism Diagnostic Interview-Revised (ADI-R), a semi-structured clinical instrument for assessing autism based on DSM-IV criteria (Lord et al., 1994), and b) autism samples from the National Institute for Mental Health (NIMH) Center for Collaborative Genetic Studies, which is largely composed of samples from the Autism Genetic Resource Exchange (AGRE) collection (Geschwind et al., 2001). We

sequenced up to 392 probands from the SSC, and up to 585 probands from the AGRE/NIMH collection. For variants of interest, we also sequenced parents if available. DNA from lymphoblastoid cell lines was obtained from the Rutgers DNA repository.

### *Controls*

Subjects not screened for autism were recruited by the survey research company (Knowledge Networks, Inc., Menlo Park, CA) from a nationally-representative internet-based panel that was selected by random digit dialing (Sanders et al., 2010). Subjects completed an online version of the Composite International Diagnostic Interview-Short Form (CIDI-SF) for lifetime history of anxiety, mood, and substance use disorders. This screen does not assess autism. Subjects consented to anonymization and deposition of their clinical information and DNA in the NIMH repository for use in any medical research. DNA from lymphoblastoid cell lines was obtained from the Rutgers DNA repository. For simplicity of comparison between experimental and control cohorts, only Caucasian samples were analyzed for both groups. NIMH control samples were sequenced or genotyped for 17 variants reported in Tables S1 and S2, as well as 4 variants from Tables S3 and S4 in the Supplemental Text. Of the 21 variants, 20 were genotyped using the iPlex assay on a MASSArray system (Sequenom) according to manufacturer's directions. Genotyping was carried out at the UCSF Cancer Core Facility. Of the 20 SNPs, 18 met call rate thresholds for inclusion. A single SNP failed iPlex design and was assayed by Sanger sequencing.

### *Mutation analysis*

Sequencing of *NPAS1* and *NPAS3* was based on gene structure information downloaded from the UCSC genome browser (hg18 assembly, NCBI build 36). We targeted exons, flanking intronic sequences, and conserved intronic regions. PCR

primers were designed using Primer3 (Rozen and Skaletsky, 2000). Primer sequences are available upon request. Sanger sequencing was performed, and samples were electrophoresed on a 3730xl DNA Analyzer capillary electrophoresis platform (Applied Biosystems). Sequencher (Gene Codes, Ann Arbor, MI) was used to edit called bases.

## **Supplemental Text**

### **DNA Sequence Analysis of *NPAS1* and *NPAS3* in Humans with Autism Spectrum**

#### **Disorders and Controls**

We carried out mutation screening of exonic, flanking intronic, and 5' and 3' untranslated regions (UTR) for *NPAS1* and *NPAS3* in up to 947 Caucasian autism probands and found 10 non-synonymous variants in *NPAS1* and seven in *NPAS3*. Sixteen of these were rare, and we assayed 13 of those in 190 control subjects unscreened for autism and found that five of seven in *NPAS1* and all six in *NPAS3* were absent in the controls.

#### **Results**

*NPAS1*: Ten non-synonymous SNPs were identified in *NPAS1*. According to both PolyPhen-2 and SIFT algorithms (Adzhubei et al., 2010; Kumar et al., 2009), the majority of the non-synonymous *NPAS1* variants are likely to be deleterious (Table S4). We did not observe two *NPAS1* non-synonymous SNPs previously deposited in dbSNP (rs1131303, rs1050741), although neither of these were discovered in population surveys following their discovery by EST alignments, nor were they in 1000 Genomes Project data. Predicted alignments to other vertebrates (see below), suggests strong conservation of most mutated amino acids. Out of the 10 mutations found in probands, six are predicted to be deleterious by PolyPhen-2 and/or SIFT, excluding the single observed stop codon. Seven were singleton mutations, while T289M and S331X were observed twice, and R308H and V424M were each observed in three individuals. Based on sequencing of available parent samples, we did not observe *de novo* non-synonymous mutations, with the exception of S331X, which was *de novo* in one of two families. The segregation of S331X was not shared between the affected siblings. Fourteen additional synonymous coding variants or untranslated region variants were observed, with only two having minor allele frequencies > 0.05 (Table S6).

*NPAS3*: Seven non-synonymous SNPs were identified in *NPAS3* in the SSC sample. As with *NPAS1*, most mutations were predicted to be deleterious by either SIFT or PolyPhen-2, although only one mutation was concordant in prediction (Table S5). We did observe a common non-synonymous variant, rs12434716 (A520P), at a frequency similar to that in a sequencing study of *NPAS3* in schizophrenia (Macintyre et al., 2010). Three variants were singleton mutations, while S458F and P466S were observed twice, and T290P and was found in nine individuals (eight heterozygotes and one homozygote). Six additional synonymous coding variants or untranslated region variants were observed, all with minor allele frequencies > 0.05 (Table S7).

*Evaluation of NPAS1 and NPAS3 gene variants in screened subjects*: To assess the frequency of the discovered variants in an ethnically similar sample, we genotyped 190 Caucasian subjects screened for major mental disorders (with the exception of autism) who are part of an NIMH-sponsored sample repository (Sanders et al., 2010). Of the 17 variants in Tables S1 and S2, we were able to successfully assay 14 variants in the controls. The single common variant (A520P in *NPAS3*, rs12434716) was seen at the same frequency in controls and cases (Table S5). For the 13 rare non-synonymous SNPs examined, five of seven in *NPAS1* were not observed in controls, while none of six in *NPAS3* were detected in the control subjects. Four synonymous or untranslated variants were genotyped, and were observed at rates similar to that seen in the cases (Tables S3 and S4).

**Alignment of non-synonymous *NPAS1* and *NPAS3* variants.** Predicted protein alignments are shown for 17 non-synonymous SNPs based on genome alignments. Human sequence is underlined, with the human reference allele bolded and highlighted in gray. Variants in other species that differ from the human are highlighted in yellow.

Human genome build: hg18

### ***NPAS1***

R124H: chr19:52,227,375-52,227,404

Human	<u>APGR<b>R</b>GPAAL</u>
Chimp	APGR <b>R</b> GPAAL
Orangutan	APGR <b>R</b> GPAAL
Rhesus	gPGR <b>R</b> GPAAL
Marmoset	APGR <b>R</b> GPAAL
Mouse	APGR <b>R</b> GPvAL
Rat	APGR <b>R</b> GavAL
Pika	APGR <b>R</b> GPAAL
Dolphin	APGR <b>R</b> GPvAL
Cow	APGR <b>R</b> GPvAL
Horse	APGR <b>R</b> GPAAL
Dog	APGh <b>R</b> GPmAL
Megabat	APGR <b>R</b> GPvAL

V213I: chr19:52,231,161-52,231,193

Human	PTPPS <b>V</b> SSSSS
Chimp	PTPPS <b>V</b> SSSSS
Orangutan	PTPPS <b>V</b> SSSSS
Rhesus	PTPPS <b>V</b> SSSSS
Marmoset	PTPPS <b>V</b> SSSSS
Mouse Lemur	PTPPS <b>V</b> SSSSS
Tree Shrew	PTPPS <b>V</b> SSSSS
Mouse	PTPPS <b>V</b> SSSSS
Rat	PTPPS <b>V</b> SSSSS
Guinea Pig	PTPPS <b>V</b> SSSSS
Dolphin	P-PPS <b>V</b> pSSSS
Cow	PTPPS <b>V</b> pSSSS
Horse	PTPPS <b>V</b> pSSSS
Cat	PTPPS <b>V</b> pSSSS
Dog	PTPPS <b>V</b> pSSSS
Megabat	PTPPS <b>V</b> pSSSS
Shrew	PTPPS <b>V</b> pSSSn
Elephant	PTPPS <b>i</b> SSSSS
Tenrec	PTPs <b>i</b> SSSSS
Armadillo	PTPPS <b>s</b> SSSSS
Opossum	gaPly <b>g</b> pSSSS

T289M: chr19:52,234,550-52,234,582

Human	VALGH <b>T</b> LPAP
Chimp	VALGH <b>T</b> LPAP
Orangutan	VALGH <b>T</b> LPAP
Rhesus	VALGH <b>T</b> LPAP
Marmoset	VALGH <b>T</b> LPAP
Tree Shrew	VALGH <b>T</b> LPAP
Mouse	VALGH <b>T</b> LPAP
Rat	VALGH <b>T</b> LPAP
Squirrel	VALGH <b>T</b> LPAP
Dolphin	VALGH <b>T</b> LPAP
Cow	VALGH <b>T</b> LPAP
Horse	VALGH <b>T</b> LPAP
Cat	VALGH <b>T</b> LPAP
Dog	VALGH <b>T</b> LPAP
Megabat	VALGH <b>T</b> LPAP
Shrew	VALGH <b>T</b> LPAP
Opossum	VALGH <b>T</b> LPAP
Tetraodon	VALaH <b>T</b> LPst
Fugu	VvLaH <b>T</b> LPst
Stickleback	VALaH <b>T</b> LPst
Medaka	VALaH <b>T</b> LPst
Lamprey	VALaH <b>a</b> LPpt

R308H: chr19:52,234,607-52,234,639

Human	HMIVF <b>R</b> LSLGL
Chimp	HMIVF <b>R</b> LSLGL
Orangutan	HMIVF <b>R</b> LSLGL
Rhesus	HMIVF <b>R</b> LSLGL
Marmoset	HMIVF <b>R</b> LSLGL
Tree Shrew	HMIVF <b>R</b> LSLGL
Mouse	HMIVF <b>R</b> LSLGL
Rat	HMIVF <b>R</b> LSLGL
Squirrel	HMIVF <b>R</b> LSLGL
Dolphin	HMIVF <b>R</b> LSLGL
Cow	HMIVF <b>R</b> LSLGL
Horse	HtIVF <b>R</b> LSLGL
Cat	HMIVF <b>R</b> LSLGL
Dog	HMIVF <b>R</b> LSLGL
Megabat	HMIVF <b>R</b> LSLGL
Opossum	HtlV <b>F</b> RLSLaL
Platypus	HMfV <b>l</b> RvhLdL
Tetraodon	HMfV <b>F</b> RvnmdL
Fugu	HMfV <b>F</b> RvnmdL
Stickleback	qMfV <b>F</b> RvnmdL
Medaka	HMfV <b>F</b> RvnmdL
Lamprey	HMfVt <b>R</b> vSLeL

S331X: chr19:52,235,555-52,235,587

Human	MDLGP <b>S</b> ELVGR
Chimp	MDLGP <b>S</b> ELVGR
Orangutan	MDLGP <b>S</b> ELVGR
Rhesus	MDLGP <b>S</b> ELVGR
Marmoset	MDLGP <b>S</b> ELVGR
Tarsier	MDLGP <b>S</b> ELVGR
Tree Shrew	MDLGP <b>S</b> ELVGR
Mouse	MDmGP <b>S</b> ELVGR
Rat	MDmGP <b>S</b> ELVGR
Guinea Pig	MDLGP <b>S</b> ELVGR
Squirrel	MDLGP <b>S</b> ELVGR
Dolphin	MDLGP <b>S</b> ELVGR
Cow	MDLGP <b>S</b> ELVGR
Horse	MDLGP <b>S</b> ELVGR
Dog	MDLGP <b>S</b> ELVGR
Megabat	MDLGP <b>S</b> ELVGR
Elephant	MDLGP <b>S</b> ELVGR
Armadillo	MDLGP <b>S</b> ELVGR
Opossum	MDvGP <b>S</b> ELiGR
Platypus	MDLGP <b>S</b> ELVGR
Lizard	MDLcs <b>S</b> ELVGk
Tetraodon	MDLtPa <b>a</b> EvVGh
Fugu	MDLtPa <b>a</b> EviGh
Stickleback	MDLtPa <b>a</b> EvVGh
Medaka	MDLtPa <b>a</b> EvVGh
Zebrafish	MDLsPa <b>a</b> EvVGh
Lamprey	lDfaa <b>e</b> ELVGk

**A422P and V424M: chr19:52,237,939-52,237,977**

Human	AFQLP <b>A</b> SVACEEA
Chimp	AFQLP <b>A</b> SVACEEA
Orangutan	AFQLP <b>A</b> SmACEEA
Rhesus	AFQLP <b>A</b> SVACEEA
Marmoset	AFQLP <b>A</b> Sm <b>t</b> CEdA
Mouse	AFQLP <b>A</b> i <b>V</b> sqEEp
Rat	AFQLP <b>A</b> i <b>V</b> sqEEs
Guinea Pig	tFQLP <b>A</b> St <b>i</b> CEdv
Squirrel	AFQLP <b>A</b> SVpCEdt
Dolphin	AFQLP <b>A</b> SVAhEdt
Cow	AFQLP <b>A</b> SVArEdA
Horse	AFQLP <b>A</b> SVACEdt
Dog	AFQLP <b>A</b> SVACEdi
Microbat	AFQLP <b>A</b> SaArEdv
Megabat	AFQLP <b>A</b> raACEdm
Armadillo	AFQLP <b>A</b> SeACEap
Opossum	AFQLP <b>r</b> tg <b>p</b> qEdl
Platypus	vFQLP <b>g</b> tgApadp

**A526E: chr19:52,240,537-52,240,569**

Human	PTLLH <b>A</b> GFLPP
Orangutan	PTLLH <b>A</b> GFLPP
Rhesus	PaLLH <b>A</b> GFLPP
Marmoset	PTLLH <b>A</b> GFLPP
Mouse	PaLLH <b>A</b> GFLPP
Rat	PaLLH <b>A</b> GFLPP
Guinea Pig	PaLLp <b>A</b> GFLPP
Dolphin	PsLLH <b>t</b> GFLPP
Cow	PsLLH <b>t</b> GFLPP
Horse	aaLLH <b>A</b> GFLPP
Dog	PsLLH <b>A</b> sFLPP
Elephant	PsvfH <b>v</b> GFLPP
Armadillo	PTLLH <b>A</b> GFLPP
Opossum	PaLvH <b>A</b> GyLaP

**P566L: chr19:52,240,657-52,240,689**

Human	PGPAL <b>P</b> EAfYP
Orangutan	PGPAL <b>P</b> EAfYP
Rhesus	PGPAL <b>P</b> EAfYP
Marmoset	PGPAL <b>P</b> EAfYP
Mouse	aGP <b>s</b> L <b>P</b> EAfYP
Rat	PG <b>P</b> sL <b>P</b> EAfYP
Dolphin	PGPtL <b>P</b> EAfYP
Cow	PGPAL <b>P</b> EAfYP
Horse	PGPg <b>f</b> <b>P</b> EAfYP
Dog	PGPtL <b>P</b> EAfYP
Megabat	PGPAL <b>P</b> EAfYP
Elephant	PGPA <b>r</b> <b>P</b> EAfYP
Opossum	PGPA <b>f</b> <b>P</b> dtlYP

**P580T: chr19:52,240,699-52,240,731**

Human	LPYPG <b>P</b> AGTRL
Chimp	LPYPG <b>P</b> AGTRL
Orangutan	LPYPG <b>P</b> AGTRL
Rhesus	LPYPG <b>P</b> AGTRL
Marmoset	LPYPG <b>s</b> AGTRL
Mouse	LPYPG <b>P</b> tGTRv
Rat	LPYPG <b>P</b> tGTRv
Guinea Pig	LPcsG <b>l</b> AGpRa
Dolphin	LPYPG <b>P</b> lGTRv
Cow	LPYPG <b>a</b> lGTRv
Dog	LsYPG <b>P</b> tGTRv
Megabat	LPYPG <b>P</b> tGaRv
Elephant	LPYPG <b>P</b> tGTRg

**NPAS3****T290P: chr14:33,313,390-33,313,422**

Human	<u>ALPPPT</u> INEVR
Chimp	ALPPPTINEVR
Gorilla	ALPPPTINEVR
Orangutan	ALPPPTINEVR
Rhesus	ALPPPTINEVR
Marmoset	ALPPPTINEVR
Tarsier	ALPPPTINEVR
Mouse lemur	ALPPPTINEVR
Bushbaby	ALPPPTINEVR
Tree shrew	ALPPPTINEVR
Mouse	ALPPPTINEVR
Rat	ALPPPTINEVR
Kangaroo rat	ALPPPTINEVR
Guinea pig	ALPPPTINEVR
Squirrel	ALPPPTINEVR
Rabbit	ALPPPTINEVR
Pika	ALPPPTINEVR
Dolphin	ALPPPTINEVR
Cow	ALPPPTINEVR
Horse	ALPPPTINEVR
Cat	ALPPPTINEVR
Dog	ALPPPTINEVR
Hedgehog	ALPPPTINEVR
Rock hyrax	ALPPPTINEVR
Armadillo	ALPPPTINEVR
Sloth	ALPPPTINEVR
Opossum	ALPPPTINEVR
Platypus	ALPPPTINEVR
Chicken	ALPPPTINEVR
Zebra finch	ALPPPTINEVR
Lizard	ALPPPTINEVR
X. tropicalis	ALPPPTINEVR
Tetraodon	tLPPsTlNEVR
Fugu	ALPPPTlNEVR
Stickleback	tLPPsTlNEVR
Medaka	ALPPPTINEVR
Zebrafish	ALPPPTINEVR
Lamprey	ALPPPTlsEiR

**S458F:chr14:33,338,717-33,338,749**

Human	<u>EKGNQ</u> SENSED
Chimp	EKGNQSENSED
Orangutan	EKGNQSENSED
Rhesus	EKGNQSENSED
Marmoset	EKGNQSENSED

Mouse lemur	EKGNh <b>S</b> ENSED
Bushbaby	EKGNh <b>S</b> ENSED
Tree shrew	EKGNQ <b>S</b> ENSED
Mouse	EKGNQ <b>S</b> ENSED
Rat	EKGNQ <b>S</b> ENSED
Kangaroo rat	EKGNQ <b>S</b> ENSED
Guinea pig	EKGNQ <b>S</b> ENSED
Dolphin	EKGNQ <b>S</b> ENSED
Cow	EKGNQ <b>S</b> ENSED
Microbat	EKGNQ <b>S</b> ENSED
Elephant	EKGNQ <b>S</b> ENSED
Tenrec	EKGNQ <b>S</b> ENSED
Armadillo	EKGNx <b>S</b> ENSED
Opossum	EKGNQ <b>S</b> ENSED
Platypus	EKGNQ <b>S</b> ENSED
Chicken	EKGNQ <b>S</b> ENSED
Zebra finch	EKGNQ <b>S</b> ENSED
Lizard	EKGNQ <b>S</b> ENSED
X. tropicalis	gKGNh <b>S</b> EqSED
Medaka	EKiqh <b>p</b> Egdae
Zebrafish	gKnqs <b>S</b> ENSED

**P466S:chr14:33,338,741-33,338,773**

Human	<u>SEDPE<b>P</b>DRKKS</u>
Chimp	SEDPE <b>P</b> DRKKS
Orangutan	SEDPE <b>P</b> DRKKS
Rhesus	SEDPE <b>P</b> DRKKS
Marmoset	SEDPE <b>P</b> DRKKS
Mouse lemur	SEDPE <b>P</b> DRKKS
Bushbaby	SEDPE <b>P</b> DRKKS
Tree shrew	SEDPE <b>P</b> DRKKS
Mouse	SEDPE <b>P</b> DRKKS
Rat	SEDPE <b>P</b> DRKKS
Kangaroo rat	SEDPE <b>P</b> DRKKS
Guinea pig	SEDPE <b>P</b> DRKKS
Dolphin	SEDPE <b>P</b> DRKKS
Cow	SEDPE <b>P</b> DRKKS
Horse	SEDPE <b>P</b> DRKKS
Microbat	SEDPE <b>P</b> DRKKS
Elephant	SEDPE <b>P</b> DRKKS
Tenrec	SEDPE <b>P</b> DRKKS
Armadillo	SEDsE <b>P</b> DRKKS
Opossum	SEDPE <b>s</b> DRKKS
Platypus	SEDPE <b>P</b> DRKKS
Chicken	SEDPE <b>s</b> DRKKS
Zebra finch	SEDPE <b>s</b> DRKKS
Lizard	SEDPE <b>s</b> DRKKS

X. tropicalis	SEDhE <b>P</b> DhKqp
Fugu	rEDPE <b>a</b> DRKqp
Medaka	daePE <b>l</b> DgnqS
Zebrafish	SEDPE <b>a</b> DsKqt

**A520P:chr14:33,338,903-33,338,935**

Human	FGALG <b>A</b> MQIKV
Chimp	FGALG <b>p</b> MQIKV
Orangutan	FGALG <b>p</b> MQIKV
Rhesus	FGALG <b>p</b> MQIKV
Marmoset	FGALG <b>p</b> MQIKV
Mouse lemur	FGALG <b>p</b> MQIKV
Bushbaby	FGALG <b>p</b> MQIKV
Tree shrew	FGALG <b>p</b> MQIKV
Mouse	FGALG <b>s</b> MQIKV
Rat	FGALG <b>p</b> MQIKV
Kangaroo rat	FGALG <b>p</b> MQIKV
Guinea pig	FGALG <b>p</b> MQIKV
Dolphin	FGALG <b>p</b> MQIKV
Cow	FGALG <b>r</b> MQIKV
Dog	FGALG <b>p</b> MhIKV
Elephant	FGALG <b>p</b> MQIKV
Tenrec	FGALG <b>p</b> MrIKa
Armadillo	FsALG <b>l</b> MQIKV
Opossum	FGtLG <b>s</b> MQIKV
Platypus	FGpLG <b>A</b> MQIKV
Chicken	FGtLG <b>s</b> MQIKV
Zebra finch	FGtLG <b>s</b> MQIKV
Lizard	FGtLG <b>s</b> MQIKV
X. tropicalis	ldALG <b>p</b> MhIKV
Tetraodon	lGgLG <b>A</b> ihIKV

**G555A:chr14:33,339,008-33,339,040**

Human	DSDSAG <b>E</b> EAGAQ
Chimp	DSDSAG <b>E</b> EAGAQ
Orangutan	DSDSAG <b>E</b> EAGAQ
Rhesus	DSDSAG <b>E</b> EAGAQ
Marmoset	DSDSAG <b>E</b> EAGAQ
Mouse lemur	DSDSAG <b>E</b> EAGAQ
Bushbaby	DSDSAG <b>E</b> EAGAQ
Tree shrew	DSDSAG <b>E</b> EAGAQ
Mouse	DSDS <b>A</b> nEAGAQ
Rat	DSDS <b>A</b> tEAGAQ
Kangaroo rat	DSDSAG <b>E</b> EAGAQ
Guinea pig	DSDSAG <b>E</b> EAGAQ
Dolphin	DSDSAG <b>E</b> EAGAQ
Cow	DSDSAG <b>E</b> EAGAQ

Dog	DSDSAGEAGAQ
Elephant	DSDSAGEAGAQ
Tenrec	DSDgAGEAGAh
Opossum	DSDSAGEAsAQ
Platypus	DSDSAaEAGpQ
Chicken	DSDSAGEvnAQ
Zebra finch	DSDSAGEvnAQ
Lizard	DSDSAGEgdAQ
Tetraodon	eeeggrdgGlp
Medaka	DeDeAeggegQ
Zebrafish	edDvedseGlQ

**S587R:chr14:33,339,104-33,339,136**

Human	RRRLSSASSPG
Chimp	RRRLSSASSPG
Orangutan	RRRLSSASSPG
Rhesus	RRRLSSASSPG
Marmoset	RRRLSSASSPG
Mouse lemur	RRRLSSASSPG
Bushbaby	RRRLSSASSPG
Tree shrew	RRRLSSASSPG
Kangaroo rat	RRRLSSASSPG
Guinea pig	RRRLSSASSPG
Dolphin	RRRLSSASSPG
Cow	RRRLSSASSPG
Dog	RRRLSSASSPG
Elephant	RRRLSSASSPG
Tenrec	RRRLSSASSPG
Opossum	RRRLSStSSPn
Platypus	RRRLSSASSPG
Chicken	RRRLSStSSPn
Zebra finch	RRRLSStSSPn
Lizard	RRRLSStSSPn
X. tropicalis	RRRLSggSSPG
Tetraodon	RlRiStspgPv
Fugu	RlRiStspSPi
Medaka	RlRLStppSPv

**A892T:chr14:33,340,019-33,340,051**

Human	SNGIHAAQTLE
Chimp	SNGIHAAQTLE
Orangutan	SNGIHAAQTLE
Rhesus	SNGIHAAQTLE
Marmoset	SNGIHAAQTLE
Bushbaby	SNGIHAAQTLE
Tree shrew	SNGIHAAQTLE
Mouse	SNGIHAAQTLE

Rat	SNGIH <b>AA</b> QTLE
Guinea pig	SNGIH <b>AA</b> QTLE
Dolphin	SNGIH <b>AA</b> QTLE
Cow	SNGIH <b>AA</b> QTLE
Horse	SNGIH <b>AA</b> QTLE
Dog	SNGIH <b>AA</b> QTLE
Shrew	SNGIH <b>AA</b> QaLE
Elephant	SNGIH <b>AA</b> QTLE
Tenrec	SNGlH <b>AA</b> QTLE
Armadillo	SNGIH <b>AA</b> QTLE
Sloth	SNGIH <b>AA</b> QTLE
Opossum	SNGIH <b>t</b> tQTLE
Platypus	SNGIH <b>AA</b> QTLE
Chicken	SNGIH <b>t</b> tQTLE
Zebra finch	SNGIH <b>t</b> tQTLE
Lizard	SNGIH <b>AA</b> QTLE
X. tropicalis	SNGIH <b>AA</b> QTLE

**A rare mutation in *NPAS1* leads to a stop codon.** Segregation of the mutations in the two families in which the variant was discovered. Clinical status of parents is unknown. Squares represent males, circles represent females. Black shading indicates individuals with ASD. The mutated allele is a C.

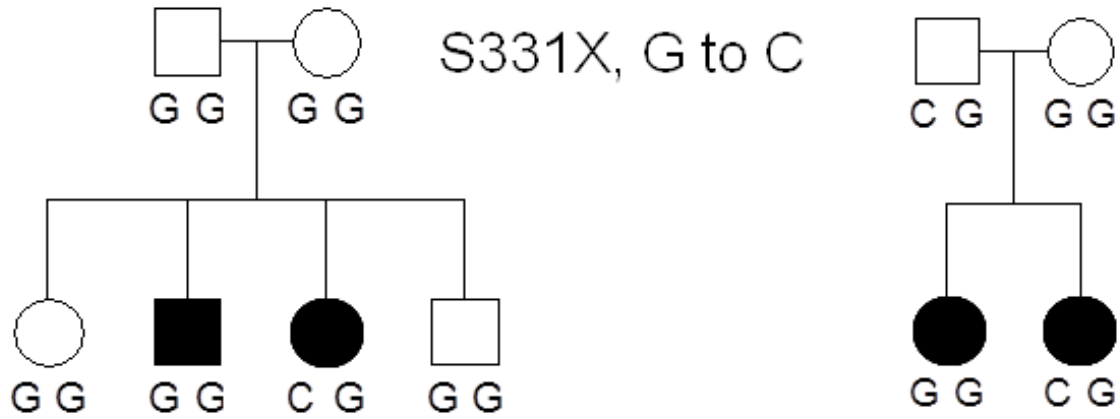


**Table S4. Rare non-synonymous coding variants in *NPAS1*.**

<b>Exon</b>	<b>hg18 Position</b>	<b>N</b>	<b>SNP</b>	<b>Minor</b>	<b>Major</b>	<b>MAF</b>	<b>Effect</b>	<b>SIFT</b>	<b>PolyPhen-2</b>	<b>Ctrl MAF</b>
4	52227388	701	R	A	G	0.0007	R124H†	TOLERATED	PROBABLY DAMAGING	0.008
6	52231176	391	R	A	G	0.0013	V213I	TOLERATED	BENIGN	0.00
8	52234566	713	Y	C	T	0.0014	T289M‡	DAMAGING	PROBABLY DAMAGING	-
8	52234623	713	R	A	G	0.0021	R308H	DAMAGING	PROBABLY DAMAGING	0.003
9	52235571	947	S	G	C	0.0005	S331X	n/a	n/a	0.00
11	52237954	898	S	C	G	0.0006	A422P	TOLERATED	BENIGN	0.00
11	52237960	898	R	A	G	0.0017	V424M§	TOLERATED	BENIGN	0.00
12	52240553	700	M	A	C	0.0007	A526E¶	DAMAGING*	BENIGN	-
12	52240673	700	Y	T	C	0.0007	P566L	DAMAGING*	PROBABLY DAMAGING	-
12	52240714	700	M	A	C	0.0007	P580T	DAMAGING*	BENIGN	0.00

hg18 Position, base pair position on UCSC genome browser build hg18; MAF, minor allele frequency; Ctrl MAF, minor allele frequency in 190 NIMH controls; \*, low confidence prediction, as prediction is based on closely related sequences; -, failed assay design; †, rs138366096 in dbSNP; ‡, rs149310092 in dbSNP; §, rs151177532 in dbSNP; ¶, rs201846524 in dbSNP.

**Table S5. Rare non-synonymous coding variants in *NPAS3*.**

<u>Exon</u>	<u>hg18 Position</u>	<u>N</u>	<u>SNP</u>	<u>Minor</u>	<u>Major</u>	<u>MAF</u>	<u>Effect</u>	<u>SIFT</u>	<u>PolyPhen-2</u>	<u>Ctrl MAF</u>
8	33313405	331	M	C	A	0.015	T290P	DAMAGING	BENIGN	0.00
12	33338733	337	Y	T	C	0.006	S458F	DAMAGING*	POSSIBLY DAMAGING	0.00
12	33338756	337	Y	T	C	0.006	P466S	DAMAGING*	BENIGN	0.00
12	33338918	338	S	C	G	0.183	A520P†	TOLERATED	BENIGN	0.17
12	33339024	338	S	C	G	0.001	G555A	TOLERATED	BENIGN	0.00
12	33339121	338	S	G	C	0.001	S587R	DAMAGING*	BENIGN	0.00
12	33340034	323	R	A	G	0.002	A892T	DAMAGING*	BENIGN	0.00

hg18 Position, base pair position on UCSC genome browser build hg18; MAF, minor allele frequency; Ctrl MAF, minor allele frequency in 190 NIMH controls; \*, low confidence prediction, as prediction is based on closely related sequences; †, rs12434716 in dbSNP.

**Table S6. Synonymous coding and untranslated variants in *NPAS1*.**

<u>Exon</u>	<u>hg18 Position</u>	<u>N</u>	<u>SNP</u>	<u>Minor</u>	<u>Major</u>	<u>MAF</u>	<u>dbSNP</u>	<u>Effect</u>	<u>Ctrl MAF</u>
5'UTR	52215991	332	R	A	G	0.017	-	UTR	
2	52216234	388	S	G	C	0.005	rs28578816	P to P	0.000
3	52216751	392	Y	T	C	0.003	rs146818939	R to R	
3	52216914	159	Y	T	C	0.003	-	L to L	
4	52227395	377	Y	T	C	0.003	rs143921498	P to P	
6	52231106	391	R	A	G	0.003	-	G to G	
9	52235614	946	R	G	A	0.295	rs3745615	Q to Q	0.276
11	52237944	567	Y	T	C	0.002	-	F to F	
11	52237998	331	Y	T	C	0.002	-	P to P	
12	52240437	345	R	A	G	0.001	rs142357211	P to P	
12	52240518	699	R	G	A	0.401	rs889169	A to A	0.413
12	52240524	354	M	A	C	0.003	-	P to P	
12	52240593	355	Y	T	C	0.001	-	P to P	
3'UTR	52240789	345	S	C	G	0.001	-	UTR	

hg18 Position, base pair position on UCSC genome browser build hg18; MAF, minor allele frequency; dbSNP, variant ID in dbSNP; Ctrl MAF, minor allele frequency in 190 NIMH controls.

**Table S7. Synonymous coding and untranslated variants in *NPAS3*.**

<u>Exon</u>	<u>hg18 Position</u>	<u>n</u>	<u>SNP</u>	<u>Minor</u>	<u>Major</u>	<u>MAF</u>	<u>dbSNP</u>	<u>Effect</u>	<u>Ctrl MAF</u>
2	32754271	329	M	C	A	0.002	-	A91A	0.003
6	33215335	333	Y	T	C	0.002	rs144972549	P242P	
8	33313386	331	R	A	G	0.002	rs140384278	A283A	
12	33339934	323	Y	T	C	0.002	-	S858S	
3' UTR	33340515	328	W	A	T	0.011	rs28658465	UTR	
3' UTR	33340555	328	InDel	-	A	0.002	-	UTR	

hg18 Position, base pair position on UCSC genome browser build hg18; MAF, minor allele frequency; dbSNP, variant ID in dbSNP; Ctrl MAF, minor allele frequency in 190 NIMH controls.

## **Supplemental References**

Adzhubei, I.A., Schmidt, S., Peshkin, L., Ramensky, V.E., Gerasimova, A., Bork, P., Kondrashov, A.S., and Sunyaev, S.R. (2010). A method and server for predicting damaging missense mutations. *Nat Methods* 7, 248-249.

Fischbach, G.D., and Lord, C. (2010). The Simons Simplex Collection: a resource for identification of autism genetic risk factors. *Neuron* 68, 192-195.

Geschwind, D.H., Sowinski, J., Lord, C., Iversen, P., Shestack, J., Jones, P., Ducat, L., and Spence, S.J. (2001). The autism genetic resource exchange: a resource for the study of autism and related neuropsychiatric conditions. *Am J Hum Genet* 69, 463-466.

Jeong, J., Li, X., McEvilly, R.J., Rosenfeld, M.G., Lufkin, T., and Rubenstein, J.L. (2008). Dlx genes pattern mammalian jaw primordium by regulating both lower jaw-specific and upper jaw-specific genetic programs. *Development* 135, 2905-2916.

Kumar, P., Henikoff, S., and Ng, P.C. (2009). Predicting the effects of coding non-synonymous variants on protein function using the SIFT algorithm. *Nat Protoc* 4, 1073-1081.

Lord, C., Rutter, M., and Le Couteur, A. (1994). Autism Diagnostic Interview-Revised: a revised version of a diagnostic interview for caregivers of individuals with possible pervasive developmental disorders. *J Autism Dev Disord* 24, 659-685.

Rozen, S., and Skaletsky, H. (2000). Primer3 on the WWW for general users and for biologist programmers. *Methods Mol Biol* 132, 365-386.

Sanders, A.R., Levinson, D.F., Duan, J., Dennis, J.M., Li, R., Kendler, K.S., Rice, J.P., Shi, J., Mowry, B.J., Amin, F., *et al.* (2010). The Internet-based MGS2 control sample: self report of mental illness. *Am J Psychiatry* 167, 854-865.